THE JOURNAL OF PHYSICAL CHEMISTRY A

 VOLUME 106, NUMBER 27, JULY 11, 2002

FEATURE ARTICLE

Closing the Loop on Bond Selective Chemistry Using Tailored Strong Field Laser Pulses

R. J. Levis*

Department of Chemistry, Wayne State University, Detroit, Michigan 48202

H. A. Rabitz*

Department of Chemistry, Princeton University, Princeton, New Jersey 08544

Received: September 12, 2001; In Final Form: January 28, 2002

Strong field, closed-loop control of gas-phase photochemical reactivity is the focus of this article. The control of chemical reactivity is now possible using tailored laser pulses to circumvent previous laser bandwidth limitations. As an illustration of this capability, ketone rearrangements and dissociation reactions are considered. To introduce the experiments we discuss both optimal control theory (OCT) and optimal control experiments (OCE) with an emphasis on closed-loop control methods using near-infrared fs pulses. Because the experiments are in the strong field regime, we present the current state of the understanding of the electronic and nuclear photophysical processes that occur when polyatomic molecules are subjected to laser intensities ranging between 10^{13} and 10^{15} W cm^{-2}. Photoelectron spectroscopy measurements are presented that begin to elucidate the control mechanisms. These delineate the order of the multiphoton process, the presence of transient shifting of excited electronic state energies (on the order of 5 eV), and the phenomena of lifetime broadening of electronic states. Recent experiments probing the energy partitioning to nuclear modes are presented with an emphasis on detecting the final kinetic energy of fragment ions. The advances in laser pulse shaping technology slaved to pattern recognition learning algorithms have opened up the prospect of studying the dynamics and chemical manipulation of virtually any system that can be introduced into the closed-loop apparatus. Rather than operating under the limitation of finding the molecule to suit the laser capabilities, the closed-loop learning control procedure operating in the strong field regime now makes it possible to merely tailor the control laser to meet the molecule's dynamical capabilities in keeping with the chemical objectives. The prospects are very bright for exploring chemical reactivity with these tools.

I. Introduction

The interaction of molecules with tailored laser pulses in the strong field regime is under active exploration for optical control of chemical reactivity. For the processes described in this article, the strong field regime is reached at laser intensities in excess of 10^{12} W cm^{-2}, where substantial Stark shifting, polarization, and disturbance of the field free electronic states occurs to produce a quasi-continuum of new states in the molecule. A calibration for the magnitude of the influence of an intense laser on a molecule can be obtained by calculating the maximum amplitude of the electric field vector of the laser beam using

$$E_o = (I/\epsilon_o c)^{1/2} \quad (1)$$

where I is the intensity of the radiation, ϵ_o is the vacuum permittivity, and c is the speed of light. For example, the easily obtained intensity of 10^{14} W cm^{-2} corresponds to $E_o = 2.75$ V/Å. The result of the interaction of such a high electric field

10.1021/jp0134906 CCC: $22.00
Published on Web 06/18/2002

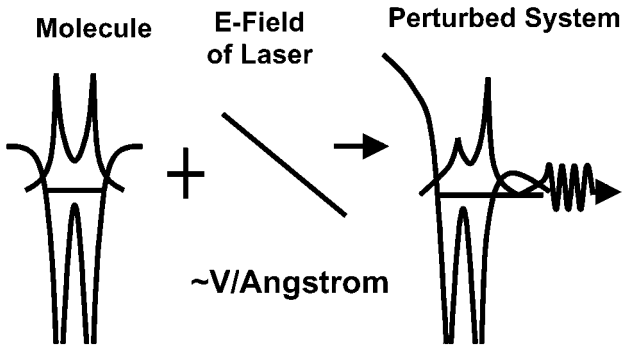

Figure 1. Schematic of a diatomic molecule interacting with an instantaneous, strong electric field. In this case the electric field strength is on the order of the field of the H_2 molecule 1 Å from the nucleus. The process shown represents tunneling of the electron into the continuum.

with a molecule is schematically shown in Figure 1 where the one-dimensional electrostatic potential energy surface of a diatomic molecule is modified by a laser pulse of approximately 1 V/Å, a field strength that is on the order of the fields binding valance electrons to nuclei. The control of the strong field-induced near continuum using closed-loop methods has been used to influence gas-phase chemical reactions[1] where the outcome of the interaction between the strong field laser and the molecule is employed to interactively discover the optimal time-dependent pulse.[2]

At first one might anticipate that the degree of chemical control using pulses of such intensity would be extremely limited due to the highly nonlinear processes induced in the molecule. However, because the pulse duration is short (~50 fs), the excitation laser has the potential to limit the intuitively expected catastrophic decomposition to atomic fragments and ions. For example, in the strong field excitation of benzene,[3] ionization of the parent species was exclusively observed up to intensities of 10^{14} W cm^{-2} with little induced dissociation. The observation of the single dominant channel (intact ionization) suggested that most of the possible final state channels (i.e., the large manifold of dissociative ionization states) may be suppressed in a well-defined, strong field intensity regime. Furthermore, at these intensities there is opportunity to substantially manipulate the molecular wave function (see Figure 1) with suitable shaping of the laser pulses to induce and manage photochemical reactivity and products.

The advent of short pulse duration, intense lasers has led to the observation of many interesting strong field phenomena in atoms, molecules, and clusters including X-ray generation from high harmonics;[4] above threshold ionization;[5] above threshold dissociation;[6] multiple electron emission from molecules;[7] intact ionization of large polyatomic molecules;[3,8,9] forced molecular rotation in an optical centrifuge;[10] production of extremely high charge states from molecular clusters;[11] production of highly energetic ions;[12] and neutrons from clusters.[13] A clear picture of the excitation mechanisms in the strong field regime is now emerging.[14] The use of this picture to understand the recent strong field, closed-loop control experiments is one focus of this review.

While the use of strong fields to control chemistry is quite new, the area of coherent control research has broad foundations.[15−17] The essence of the control concept in terms of optical fields and molecules is captured by the following transformation goal:

$$|\psi_i\rangle \rightarrow |\psi_f\rangle \tag{2}$$

where an initial quantum state $|\psi_i\rangle$ is steered to a desired final state $|\psi_f\rangle$ via interaction with some external field. As a problem in quantum control, the goal is typically expressed in terms of seeking a tailored laser electric field $\epsilon(t)$ that couples into the Schrödinger equation

$$i\hbar\frac{\partial}{\partial t}|\psi\rangle = [H_0 - \mu \cdot \epsilon(t)]|\psi\rangle \tag{3}$$

through the dipole μ. This Born−Oppenheimer picture can be expanded to explicitly consider the electrons and nuclei (cf., the discussion in section II). Regardless of the necessary level of Hamiltonian detail, the general mechanism for achieving quantum control is through the manipulation of constructive and destructive quantum wave interferences. The goal is to create maximum constructive interference in the state $|\psi_f\rangle$ according to eq 2, while simultaneously achieving maximum destructive interference in all other states $|\psi_{f'}\rangle$,$f' \neq f$ at the desired target time T. A simple analogy to this process is the traditional double slit experiment.[18] However, a wave interference experiment with two slits will lead to only minimal resolution. Thus, in the context of quantum control, two pathways can produce limited selectivity when there are many accessible final states for discrimination. Rather, a multitude of effective slits should be created at the molecular scale in order to realize high quality control into a single state,[19] while eliminating the flux into all other states.

The requirement of optimizing quantum interferences to maximize a desired product leads to the need for introducing an adjustable control field $\epsilon(t)$ having sufficiently rich structure to simultaneously manipulate the phases and amplitudes of all of the pathways connecting the initial and final states. As will be seen, construction of such a pulse is currently possible in the laboratory using the technique of spatial light modulation.[20,21] However, calculation of the time-dependent electric fields to produce the desired reaction remains a problematic issue for chemically relevant reactions. Unfortunately, the Hamiltonian at the Born−Oppenheimer level remains largely unknown for polyatomic molecules, and this severely limits the ability to perform a priori calculations at the present time. Even if the field free molecular Hamiltonian were known, the highly nonlinear nature of the strong field excitation process effectively removes all possibility of calculating an appropriate pulse shape in this regime. Thus we are left with the following conundrum: If the design can be carried out reliably, then the physical system will likely not be of much interest, while for interesting physical systems, reliable designs cannot be performed.

The method of closed-loop control for laser-induced processes[2] offers a way to surmount our lack of knowledge of the Hamiltonian to find appropriate pulse shapes, $\epsilon(t)$. In closed-loop operations, the molecule, the laser pulse shaper, and a pattern recognizing learning algorithm form the elements for repeated cyclic operation to teach the laser how to control the molecules. A schematic of this process is shown in Figure 2. This procedure, especially in the strong field regime, provides the only general means at the present time to deduce laser pulse shapes that can successfully manipulate molecular dynamics phenomena. The method is general because any molecule can be excited in the strong field regime using a nominally 800 nm pulse, and closed-loop methods provide a means to determine the optimal time-dependent, strong field excitation to produce a specific target state. The quantum system, upon each cycle of the loop, is replaced by a new one, thereby (a) avoiding the need for ultrafast computations, electronics, and laser switching, and (b) eliminating any concerns about the observation process

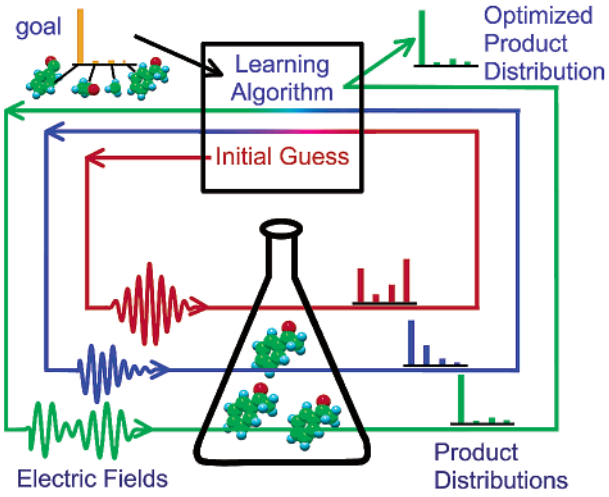

Figure 2. Representation of the concept of closed-loop control. In this case there are four possible outcomes shown for the interaction of the laser pulse with the molecule. The desired distribution of products is first input into the algorithm at the upper left of the Figure. The program creates an initial laser pulse shape that interacts with the sample and yields a product distribution. Based on experimental measurement of the distribution (typically in combination with several other experiments) the algorithm creates a new pulse that yields a new distribution. The system loops iteratively until the desired level of control is exerted.

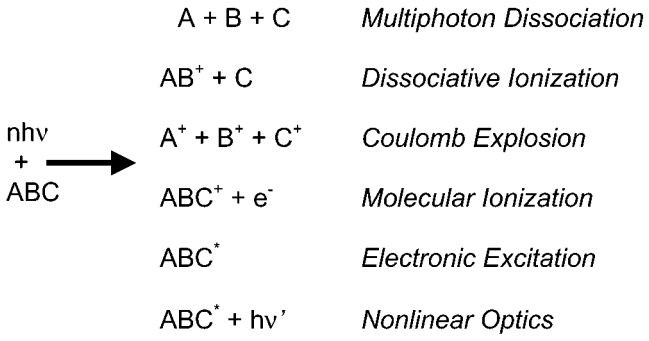

Figure 3. Potential outcomes of the interaction of intense laser radiation with a molecule. At the present time the wavelengths used for the interaction range between 10μm and 200 nm. The wavelengths employed in the studies reported here range between 750 and 850 nm with intensities of 10^{13} to 10^{15} W cm^{-2}.

disturbing the actual dynamics. In the experiments described in this article, the phase and amplitudes of the component frequencies of a 40 fs pulse are the control variables, and the resultant mass spectrum is the observable employed to evaluate the fitness of the pulse shape. Optical or other means of detection could also be employed for a feedback signal.

The closed-loop learning procedure for teaching lasers to control quantum systems has now been demonstrated in many diverse investigations. Those performed to date employ closed-loop control of a laser pulse shaper to optimize a desired process. These experiments include adaptive pulse compression[22,23] and control of pulse phase,[24] manipulation of pure rotational[25] and vibrational[26] dynamics in diatomics, one and two photon transitions in atoms,[27,28] creation of specific wave functions in Rydberg atoms,[29] and generation of high harmonics in Ar gas.[30] In the case of controlling chemical processes, a number of experiments have been performed. These include schemes employing low lying resonances to maximize fluorescence from a dye molecule in solution,[31] generation of specific photochemical fragments from organometallics[32,33] and alkali clusters,[34] maximization of stimulated Raman signal from methanol in solution,[35] and the optimization of coherent antistokes Raman emission.[36] Most recently, shaped, strong field laser pulses have been employed to enable the control of photodissociation processes in organic molecules.[1,37] The combination of closed-loop operations with strong field laser control has opened the door to the ready control of chemically interesting processes.

This paper seeks to define the emerging area of strong field control of chemical reactivity using closed-loop, tailored light pulses. To do this we review several relatively new areas of research including closed-loop optimization and strong field processes. We also review the experimental linkage of these two areas through spatial light modulation of intense laser radiation. Experiments using intense near-infrared laser pulses will be considered here. The paper is organized into the following sections. Section II reviews the processes resulting from the interaction of molecules with strong laser fields; including both electronic and nuclear dynamics. Principles of quantum optical control, and especially closed-loop learning control with tailored femtosecond laser pulses, are discussed[49] in section III. Laboratory laser control of atomic and molecular processes in the strong-field regime is the subject of section IV. Finally, section V considers future trends and possible new applications of closed-loop laser control of molecular dynamics phenomena.

II. Molecules in Intense Laser Fields

When a molecule interacts with an intense laser pulse, a number of product channels may be accessed. Some of the potential outcomes are listed in Figure 3 where coupling into the nuclear, electronic, and nonlinear optical channels are delineated. Initial intuition suggested, incorrectly, that intense, short duration laser pulses interacting with polyatomic molecules would result primarily in multiphoton dissociation as shown in the first channel. Early experiments using intense nanosecond, picosecond, and femtosecond pulses provided ample evidence for the second and third coupling channels in Figure 3, which may be described as dissociative ionization and Coulomb explosion,[38] respectively. Pulses of femtosecond duration have been shown to couple into electronic channels, resulting in ionization without nuclear fragmentation for molecules such as benzene and naphthalene.[3] In such experiments the energy in excess of the ionization potential (up to 50 eV!)[39,40] couples mainly into the kinetic energy of the photoelectron. In terms of control experiments, the ability to produce intact ions at such elevated laser intensities suggested the possibility that intense lasers could be used to guide the dynamics of a molecule into a channel other than catastrophic decomposition. Molecules interacting with intense laser fields may also convert the fundamental of the excitation laser into higher harmonics.[41] This review will focus on the channels of dissociative ionization and molecular ionization listed in Figure 3.

The relative importance of each product channel shown in Figure 3 is dictated by the Hamiltonian for the molecule−radiation system. Our understanding of the Hamiltonian for polyatomic molecules in general, and the more complex Hamiltonian for the interaction between strong fields and molecules in particular, is rather limited at the present time.[9] One would like to have high quality time-dependent calculations to model the strong field interaction, but these are simply intractable with current computational technology. Calculations for simple systems containing up to three protons and one or two electrons have been performed, and these systems are reasonably well understood.[42−44] For polyatomic systems, the

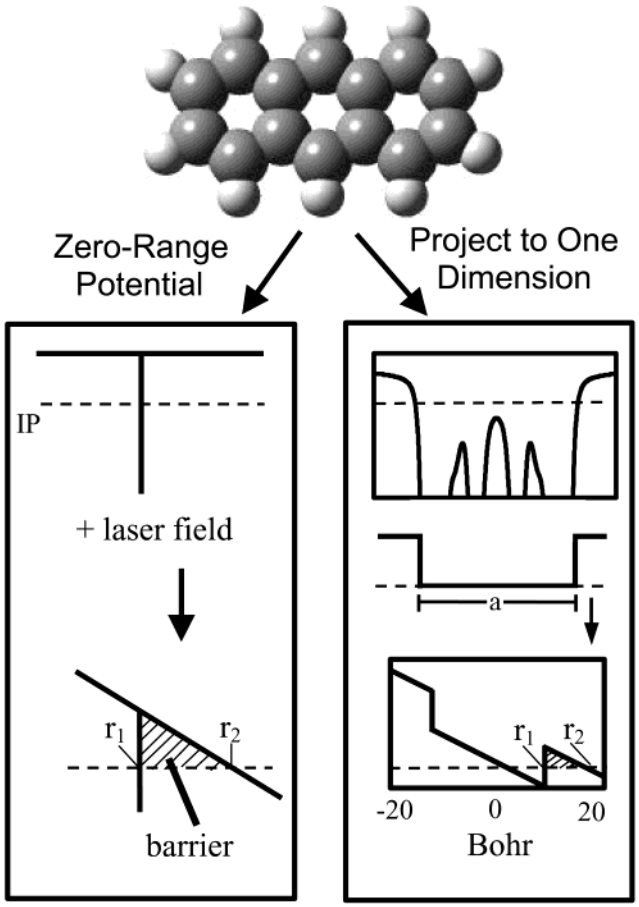

Figure 4. Schematic of the structure-based model for representing molecules in intense fields. The presentation in the left-hand panel is the zero-range model where only the ionization potential of the system is employed in calculations. The presentation in the right-hand panel represents the use of the electrostatic potential of the molecule in determining an appropriate one-dimensional rectangular well to represent the spatial extent of the system. To compare the models, an electric field of 1 V/Å is superimposed on each potential to reveal the barrier for tunnel ionization.

number of degrees of freedom is too large for first-principles calculations. Thus, simple models have been employed to gain some insight into the mechanisms of interaction between intense laser pulses and atoms.

There is a hierarchy of models for representing molecules interacting with intense laser fields. The earliest viewed the potential energy of interaction between the electron and the core as a delta function having a single state at the ionization potential of the system (called a zero-range potential).[45] Subsequently, a Coulomb potential was employed for calculations in atoms.[46,47] This was followed by a rectangular potential for molecules defined within the context of the structure-based model as shown in Figure 4.[9,39,48−50] The rectangular potential approximates the delocalization of electrons over the length scale of the molecular dimension by defining the width of the well to be equal to the characteristic length of the molecule. The characteristic length is defined as the largest distance between classical turning points in the three-dimensional electrostatic potential energy surface at the ionization potential of the molecule. The height of the rectangular well is the ionization potential of the molecule. A further advance incorporated time dependence into the radiation−molecule interaction to go beyond the quasi-static regime.[51]

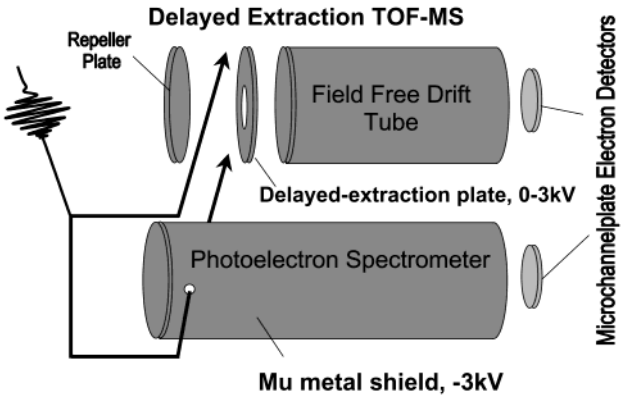

Figure 5. Schematics of the photoelectron spectrometer and the time-of-flight ion detector used for measuring the kinetic energy distribution and molecular weight of the product ions.

The experiments reviewed in this article focus on both photoelectron and photoion measurements to determine the basic phenomenology of strong field excitation of polyatomic species and to test theoretical models. The apparati used to measure the photoelectron and photoion distributions are shown in Figure 5. The electron kinetic energy distributions have been measured as a function of molecular structure and laser intensity. The photoelectron distribution provides a snapshot of the intense laser-molecule interaction during excitation because the time scale for photoelectron ejection is short (∼fs) in comparison with the time scale for photoion decomposition (∼ps). The latter provides information about the final state distribution of the laser-molecule interaction. The photoion experiments reviewed here include measurements of the ion mass distribution and ion kinetic energy distribution. The photoion kinetic energy distribution measurements compliment the photoelectron measurements regarding the final state energy partitioning after strong field excitation.

A. Electronic Dynamics of Molecules in Intense Laser Fields. To describe the mechanisms of strong field control of chemical processes it is important to consider the influence of the intense laser field on electrons in the molecule. For instance, we will see that bound electrons can gain significant ponderomotive energy (∼1−5 eV) during the pulse, and eigenstates can shift by similar energies.[52] In the case of the interaction of a laser pulse with a molecule, the appropriate starting point is the Hamiltonian for a multielectron system interacting with an electromagnetic field:

$$H = \frac{P_c^2}{2M} + \frac{1}{2\mu}\sum_{I=1}^{z} P_I^2 + \frac{1}{m_n}\sum_{i>j=1}^{z} P_i \cdot P_j + V(x_1..., x_i, ...x_c) + \frac{e}{\mu c} A(x_c, t)\frac{i=1}{Z} P_i + \frac{Ze^2}{2\mu c^2} A^2(x_c, t) \quad (4)$$

where P is momentum,V is the potential energy as a function of position, Z is the nuclear charge, and $\boldsymbol{A}(x_c,t)$ is the vector potential of the laser radiation. The first four terms describe the field free motion of the system. The last two terms describe the effect of the laser radiation on the population of eigenstates and corresponding shifts in the eigenstates of the system. In the electric field gauge the last term becomes

$$Ze^2E^2(x_c, t)/(2\,\mu\omega^2) \quad (5)$$

where E is the electric field of the laser, and ω is the frequency of the laser. The average of this term over the period of

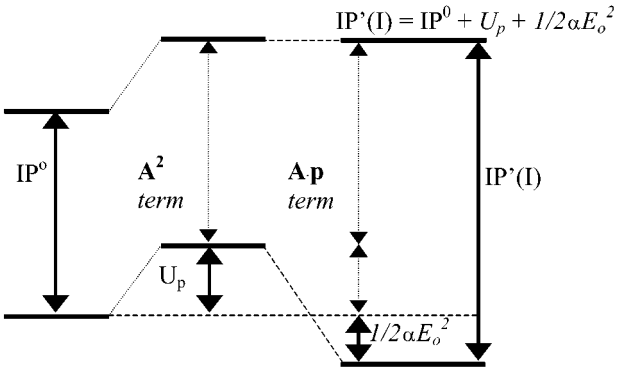

Figure 6. The effect of various terms in the Hamiltonian for a charged particle in an oscillating electromagnetic field is shown. The ionization potential of the system remains unchanged by the A^2 term as all states are raised equally. The $A \cdot P$ term lowers the ground state of the system by an amount equal to the A^2 term plus an additional amount due to the induced polarization of the system. The net result is an increase in the ionization potential by an amount approximately equal to the ponderomotive potential of the laser pulse.

oscillation for linearly polarized light is

$$U_p = (Ze^2E_0^2)/4\,\mu\omega^2) \tag{6}$$

where E_0 is the amplitude of the electric field. U_p is known as the ponderomotive potential. In strong fields this term shifts all eigenstates upward in energy equally by U_p. A differential shifting of eigenstates results from the **A·P** term. To first and higher order, the **A·P** term may used to describe allowed transitions of amplitude between eigenstates. To second and higher order, this term will describe differential shifting of the eigenstates. The magnitude and sign of the shift of a given state are dependent on the wavelength and the electronic structure of the system. Pan et al.[53] have derived expressions for the shifting of the ground state and Rydberg/continuum states of a model system. A lowest nonvanishing order perturbation theory treatment[53] yields the ground (ΔE_g) and Rydberg level (ΔE_R) energy shifts as

$$\Delta E_g = -\frac{Ze^2E_0^2}{4\mu\omega^2} - {}^1/_2\,\alpha E_0^2 \tag{7}$$

$$\Delta E_R \approx 0 \tag{8}$$

where α is the ground-state polarizability. The first term in eq 7 is the negative of the ponderomotive potential U_p. The second term is equivalent to the dc Stark shift. This treatment is valid when the ground state is deeply bound and separated from adjacent eigenstates by many times the photon energy, $h\nu$ (the low-frequency approximation). This is valid for most atoms and molecules investigated with near-infrared or longer wavelength light. High lying bound states and all continuum states experience no **A·P** shift, whereas deeply bound states of the atom experience a much greater, negative shift.[54] The pertinent shift in the states as a function of the terms in the Hamiltonian in the long wavelength limit is summarized in Figure 6.

The laser intensities employed in recent high field experimental manipulation of chemical reactivity range up to 5×10^{14} W cm^{-2}. This corresponds to ponderomotive shifts up to 10 eV with similar shifts in the separation of the ground and excited-state potential energy levels. The laser employed in these investigations has a period of 2.5 fs and an envelope with fwhm of 60−170 fs corresponding to at least a several hundred significant oscillations in the electric field vector interacting with the molecule. The states of the molecule undergo an associated oscillation in the splitting between energy levels that may result in periodic excitation on a time scale of the period of the laser. This dynamic shifting of energy levels implies that there will be transient field-induced resonances (or Freeman resonances).[55] Evidence for these resonances in the case of molecules has been obtained by measuring the strong field photoelectron spectroscopy of a number of molecules including acetone, acetylene,[52] water, benzene, and naphthalene.[56] The oscillatory nature of the intense laser excitation also leads to above threshold ionization (ATI) peaks in the photoelectron spectrum.[5] These are denoted by peaks spaced by the photon energy extending to many photons above the minimum number required for ionization.

In the case of acetylene,[52] strong field photoelectron evidence has been found for substantial shifting (1−4 eV) of the 4p series of Rydberg states to attain resonance. Peaks observed in strong field photoelectron spectra can be assigned via transient shifting of states by an amount up to the ponderomotive potential of the laser. The method developed to measure and assign the spectra is called field-induced resonance enhanced multiphoton ionization (FIRE MPI). To assign the strong field spectra one first calculates $U_p'(I)$, the variable ponderomotive shift required to bring a given candidate state into l photon resonance[52] (see Figure 6 for the field dependent shifting of states). This virtual ponderomotive shift is

$$U_p'(I) = lh\nu - E_{state} \tag{9}$$

where E_{state} is the energy of the given state under field-free conditions. $U_p'(I)$ is allowed to shift up to the maximum ponderomotive potential of the laser, U_p, because resonance may occur at any intensity within that range. The *IP* of the system at the instant of resonance is shifted simultaneously to some higher (intensity dependent) value given by

$$IP'(I) = IP + U_p'(I) \tag{10}$$

The kinetic energy of the photoelectron generated by absorbing m additional photons above the l photon resonance is then

$$E_{feature} = (l + m)h\nu - IP'(I) \tag{11}$$

In the limit where $U_p' = 0$, eq 5 reduces to the conventional REMPI condition, $E_{feature} = (l + m)h\nu - IP$, where $lh\nu = E_{state}$. However, in strong laser fields, E_{state} may shift into l photon resonance, giving rise to the transient features observed in FIRE-MPI. All potential l-photon resonances are analyzed to determine those generating photoelectrons of appropriate kinetic energy. Such field-induced shifting of intermediate states provides a powerful mechanism for strong field coupling to molecules and may be responsible in part for the strong field control mechanism. In the case of acetylene, the measurements also demonstrated that strong field photoelectron spectroscopy could detect states that had been theoretically predicted but were not detected using nanosecond resonance-enhanced multiphoton ionization because of short-lived states.

Transient resonances are not the only strong field processes induced upon molecular eigenstates during intense laser. The electric field can also broaden molecular states through a lifetime mechanism. Lifetime broadening is expected for any mechanism that causes decay of population from a given state, including, for example, ionization, nonadiabatic effects, and dissociation. In the static limit, an electric field superimposed on any system can result in tunneling. The tunneling rate may be calculated using the WKB approximation (modeling the system as one-

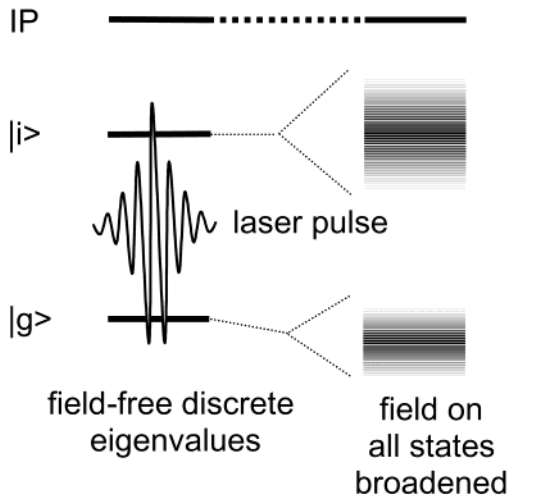

Figure 7. A schematic of the field-induced broadening resulting from a decreased lifetime of ground and excited states from ionization processes. Also shown is the field-induced shifting of the ground state to lower energy as a result of the intense laser pulse. Both of these processes contribute to an increase in the effective bandwidth in the excitation process.

dimensional) where the rate is given by

$$w = \exp\{-2\int_{r_1}^{r_2} [2(IP - V(r))]^{1/2}\, dr\} \qquad (12)$$

where the limits of integration are defined by the path length for tunneling, as shown in Figure 4. The lifetime of the molecule in the neutral state is given by the inverse of the tunnel ionization rate. Thus, an upper limit is placed on the lifetime of the neutral state which may then be related to the uncertainty of the state energy by the Heisenberg relation

$$\Delta E \Delta\, t = h \text{ or } \Delta E w^{-1} = h \qquad (13)$$

Lifetime broadening enhances the opportunity for excitation and may be thought of as a mechanism for increasing excitation bandwidth. Here, the excitation bandwidth is the combination of the laser bandwidth and the width of the field-induced quasi continuum. In the weak field regime, the excitation bandwidth is given almost exclusively by the bandwidth of the exciting laser. A long duration radiation source, such as a nanosecond laser, will have a bandwidth of $\sim\mu$eV, while a 100 fs duration laser will have a bandwidth of $\sim$50 meV. In the weak field case the excitation scheme is necessarily limited to states that fall within the spectral range of the excitation source and possibly low harmonics of that source. In the strong field case there is an opportunity to increase the bandwidth of the excitation laser by widening the eigenstate to a band of perhaps several eV by the lifetime broadening mechanism. A schematic of the combined effects of state shifting and lifetime broadening is shown in Figure 7. These strong field effects provide an attractive regime to consider for molecular control, as one no longer needs to search for a molecule that suits the finite laser frequencies available in the laboratory. Rather, the laser pulse may be tailored to suit virtually any molecule.

Evidence for the broadening of eigenstates during the strong field excitation process can be found in the photoelectron measurements for acetylene,[50] benzene, and naphthalene.[56] In each of these molecules the photoelectron spectra contain a well-defined series of features that can be assigned using the method of FIRE MPI as described previously. As the laser intensity increases above that required for detection of photoelectrons,

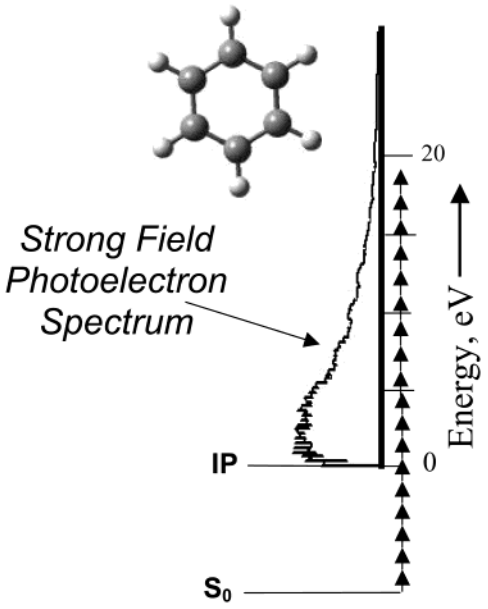

Figure 8. Strong field photoelectron spectrum for benzene shown on an energy axis that includes the photons necessary to induce ionization. The photoelectron spectrum was obtained using 2×10^{14} W cm^{-2}, 800 nm radiation of duration 80 fs. The quantum energy of the photons are shown to scale and indicate that 10−20 photons are available to drive excitation processes in the strong field excitation regime. In addition, uncertainty broadening of the pulse will also produce a distribution of allowed photon energies that approaches the photon energy when multiphoton processes of order 10 are approached.

the features begin to broaden. In general at an intensity of roughly 1 order of magnitude larger than the ionization threshold, the discrete features are smeared into a continuum. This implies that for these highly nonlinear processes broadening on the order of several eV occurs rapidly above the threshold for ionization, perhaps through the lifetime mechanism. The fact that intact ions are observed in the mass spectra at these elevated intensities suggests that ionization of dissociated products is not responsible for loss of the features. A similar broadening of eigenstates has been observed at constant laser intensity in the series benzene, naphthalene, and anthracene at constant laser intensity where the characteristic length of the molecule increases.[39] In the case of benzene, having the smallest characteristic length and hence the largest barrier to tunnel through, there are several series of observable features. In the case of naphthalene, having a larger characteristic length, there are discrete features superimposed on a feature having a broad distribution of energies. Anthracene reveals no evidence for well-resolved peaks within the broad photoelectron distribution. These observations suggest that the lifetime broadening scales with increasing characteristic length.

An important consideration for the control of chemical reactivity in the strong field regime is the order of the multiphoton process during excitation. This order indicates the maximum number of photons that are available to drive a chemical reaction. Some indication of the number of photons involved in the strong field excitation process can be gleaned from measurements of strong field photoelectron spectra. Figure 8 displays the photoelectron kinetic energy distribution for benzene with the energy axis rotated by 90 degrees. The energy scale has been offset to include the energy of the ground and ionization potential of the molecule in the absence of the strong electric field. The arrows on the figure represent the photons involved in both exceeding the ionization potential and in

creating the above threshold ionization photoelectron distribution. At least six photons are required to surmount the ionization potential of benzene. Recall that in the presence of the strong electric field, the ionization potential will increase by an amount greater than the ponderomotive potential, further increasing the actual number of photons involved in the excitation process. At the intensity of 10^{14} W cm^{-2} in this measurement, on the order of 10 photons may be absorbed to induce the photoelectron spectra shown. Including the photons required to reach the ionization potential, this means that approximately 20 photons may be involved in the excitation process. With the shaped pulses used in the experiments described in section IV, the intensities are lower and on the order of 10 or fewer photons are likely involved in the excitation process.

Several other methods have been developed to predict the ionization probability of molecules. One is based on discretizing a molecule into a collection of atomic cores that individually interact with the strong laser field and emit electrons.[57] In this model, a carbon atom, for instance, is represented by an atom with an effective potential. The ionization probability is then a function of the individual ionization probabilities from atoms with opportunity for quantum interference during the ionization event. Unfortunately, the method must be parameterized for each molecule at the present time. The second method under development employs S-matrix[57] theory to calculate the ionization probability for atoms and now molecules. This method focuses on the interference of the outgoing electron wave. Predictions about relative ionization probabilities are based on the symmetries of the highest occupied molecular orbital.

B. Nuclear Dynamics of Molecules in Intense Laser Fields. The response of a molecule to a time-dependent electric field is the means by which chemical reactivity is controlled in these experiments. In the case of weak laser fields, the response can be calculated with reasonable accuracy.[58−60] In the case of strong fields, the situation is much more complex but the dynamical possibilities are much richer. In principle, the nuclear dynamics in strong laser fields could be determined using exact numerical solutions of the time-dependent Schrödinger equation. Such solutions are possible only for the simplest of molecules at the present time.[42−44] In fact, the bulk of such simulations have been performed using a one-dimensional model for the H_2+ system.[61−63] These calculations show the presence of non-Born−Oppenheimer electron−nuclear dynamics. Since the nuclei move considerably on the time scale of the laser pulse, electronic modes are necessarily coupled with nuclear modes. Three distinct final states have been observed in strong field (no pulse shaping) mass spectra of polyatomic molecules: production of intact molecular ion, ionization with molecular dissociation, and removal of multiple electrons to produce Coulomb explosion.[9] The hallmark of the latter process is production of ions substantial (>5 eV) kinetic energy. The presence of Coulomb explosion has been shown to depend on charge resonance-enhanced ionization[64] (CREI) which becomes the dominant mechanism at large critical internuclear distances. Interestingly, the production of high charge states in molecular clusters can be controlled using pump−probe excitation schemes.[65]

At intensities that are lower than the threshold for multielectron ionization, the majority of molecules display some fraction of intact ionization. This phenomenon is not expected intuitively because the ionization processes are not resonant with low order multiples of the fundamental frequency, implying that intense pulses must be employed for excitation. Nonetheless, many molecules have been investigated to date and all appear to provide some degree of intact molecular ionization when 800 nm excitation is employed. The mechanism behind this ionization appears to involve suppression of ladder switching coupled with coherent excitation of electronic modes. The state of this subject has been reviewed recently.[9,66,67]

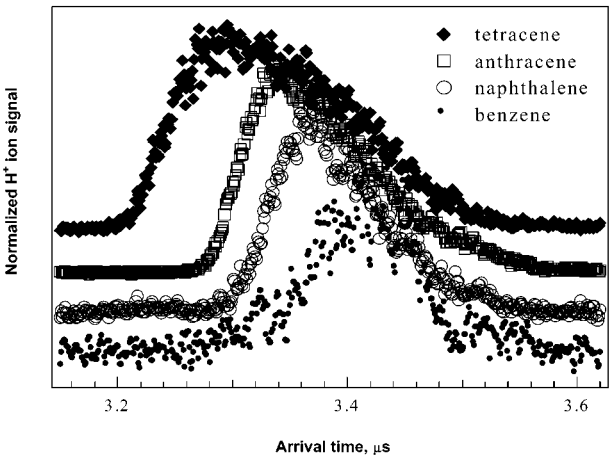

Figure 9. Retarding field measurement of the H^+ ion kinetic energy distributions arising from benzene, naphthalene, anthracene, and tetracene after excitation using 2×10^{14} W cm^{-2}, 800 nm radiation of duration 80 fs. The measurements reveal that as the characteristic length of the molecule increases, the cutoff energy increases monotonically.

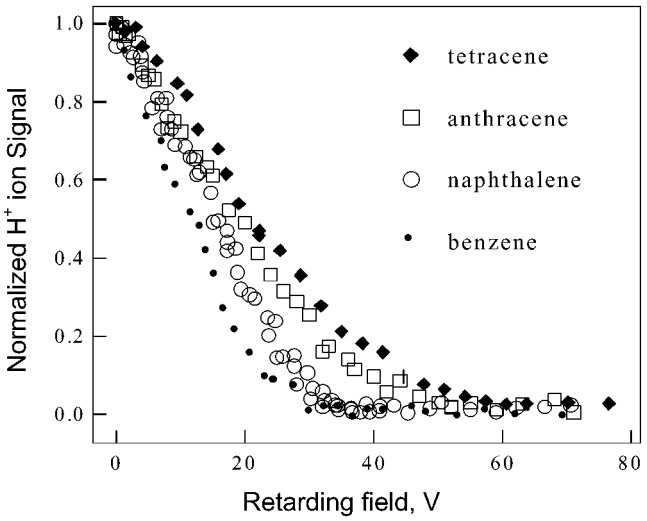

Figure 10. Time-of-arrival distributions for the H^+ ions for benzene, naphthalene, anthracene, and tetracene after excitation using 2×10^{14} W cm^{-2}, 800 nm radiation of duration 80 fs. The time of arrival distributions were measured by allowing the ions to drift in a field free zone of length 1 cm prior to extraction into the drift tube. In this experiment, earlier arrival times denote higher kinetic energies.

To measure the amount of energy that may couple into the nuclear degrees of freedom during the intense laser excitation event, we have investigated[40] the kinetic energy release in H^+ ions using both time-of-flight and retarding field measurements. A typical time-of-flight mass spectroscopy apparatus employed to make such measurements is shown in Figure 5. In the series benzene, naphthalene, anthracene, and tetracene, the most probable kinetic energy in the measured distributions was observed to increase as the characteristic length of the molecules increased as shown in Figure 9. The corresponding retarding field measurements are shown in Figure 10. Again the coupling into nuclear degrees of freedom was observed to increase in the larger molecules. The most probable kinetic energies increased from 30 V for benzene to 60 V for tetracene when a 1.2×10^{14} W cm^{-2} laser excited the molecules. In terms of

providing an enabling capability for strong field control, these results suggest that up to 80 photons may be involved in the excitation process when a molecule such as tetracene is excited under strong field conditions.

A general observation after ionization of large polyatomic molecules is the measurement of an enhanced degree of dissociation as the length of the molecule increases. This was first attributed to field-induced effects[3] without a quantitative model. Recently, a strong field nonadiabatic coupling model has been introduced to account for the enhanced coupling into nuclear modes in molecules with increasing characteristic length.[51] This excitation is akin to plasmon excitation where the precise energy of the resonance depends on the coherence length and binding energy of the electrons and the strength and frequency of the driving field. The model considers the amplitude of electron oscillation in comparison with the length of the molecule. If the amplitude of oscillation is small, the molecule may first absorb energy nonresonantly and then ionize from the excited states. The amplitude of the electron oscillation in an laser field is given by $a_{osc} = E/\omega_L^2$. In the event that the $a_{osc} < L$, where L is the characteristic length of the molecule, the electron gains ponderomotive energy from the laser. Given an energy level spacing of Δ_o, the probability of nonadiabatic excitation within the Landau−Zener model becomes $\exp(-\pi\Delta_o^2/4\omega_L EL)$. As described,[45] the threshold for nonadiabatic excitiation (when $\Delta_o^2 = \omega_L EL$) of a 4 eV transition for a system having $L = 13.5$ Å with 700 nm radiation occurs at 5.6×10^{12} W cm^{-2}. This theory implies that the probability for exciting nuclear modes in large molecules with delocalized electronic orbitals increases monotonically with characteristic length as observed experimentally.[3,51] The theory also suggests that intact molecular ionization will increase with increasing excitation wavelength for large molecules, and this has been confirmed.[51] Whether the nonadiabatic excitation can be controlled remains an open question at the present time. The present successes[1,32,37] in controlling chemical reactivity suggest that nonadiabatic processes either are not significant or that the closed-loop control method is able to effectively deal with this excitation pathway.

III. Theoretical Concepts for Controlling Molecular Dynamics Phenomena

A. General Considerations. The material in section II spelled out the phenomena and mechanisms operative when strong laser fields interact with polyatomic molecules. The present section will introduce the formal concepts and principles underying the control of molecular dynamics using such laser-induced processes. Attempts at controlling molecular-scale phenomena with lasers have a long history,[68] going back to the early 1960s. It is useful to freshly examine the basic objectives and desires while considering the special features provided by operating in the strong field regime. Perhaps the most important aspect of operating with strong fields is the ability to move the molecular energy level resonances about, as necessary, to cooperate with the laser capabilities and thereby create molecular electronic−nuclear wave packets with great flexibility.[1] An essential feature of this process is the effective broad bandwidth provided the strong field interactions with the molecule. Analogous broad bandwidth control capabilities may also emerge from other laser technologies (e.g., locking together multiple lasers operating at distinct frequencies) in the future.[69]

Regardless of the control field characteristics, a basic goal of all chemical experiments is to achieve the best possible outcome (e.g., selective manipulation of reactivity). Thus an optimization process is a desirable way to manipulate molecular-scale phenomena, thereby laying the foundation for introducing optimal control theory[70−72] (OCT) as well as the allied realization of optimal control experiments[73] (OCE). The notions of OCE, and especially its practical closed-loop implementations,[2,74−84] have roots in OCT, and both procedures share some common algorithmic features.

Given the general goal of steering the dynamics of the molecular system, the next consideration is how to identify the appropriate laser fields to meet the posed objectives. Some 40 years ago, at the inception of laser control over reactivity, simple chemical intuition was thought to be sufficient for this purpose;[68] the lack of significant positive results over the subsequent approximately 30 years speaks to the inadequacy of using intuition alone. Physical intuition will always play a central role; however, it needs to be channeled into the appropriate mathematical and laboratory frameworks to be useful. A traditional approach to discover appropriate laser fields for molecular control would be through theoretical design, followed by implementation of the design in the laboratory upon the actual molecular sample.[70,72,73,85,86] This logic, folded in with the desire to achieve the best possible results, is the essence of OCT for attaining laser field designs. Although many practical difficulties may be encountered in executing such designs for interesting chemical systems (i.e., polyatomic molecules), OCT laid the foundation for OCE[2,87] leading to the recent successful laser experiments on manipulating chemical reactivity in complex molecules[1,32] and other systems.[30,35,88,89] In addition, the largely informational inadequacies (i.e., lack of quantitative knowledge of the Hamiltonian) and computational difficulties plaguing OCT are not inherent. Algorithmic and other advances will surely lead to better design capabilities in the coming years. For all of these reasons, section IIIB will summarize the general concepts behind OCT.

Although the capability of designing laser fields to achieve particular physical objectives is improving, a most interesting set of recent experiments,[1,30−32,35,88,89] and especially those involving strong field manipulation of polyatomic molecules, have operated by performing OCE directly in the laboratory. The success of this detour around OCT fundamentally rests on the ability to perform high throughput laser control experiments,[19] slaved to fast learning algorithms capable of operating at the apparatus duty cycle. In this fashion, patterns are rapidly identified in the control field → molecular response relationship emerging from each cycle of the closed-loop operations, thereby homing in on control fields that optimally achieve the desired physical objective. Notwithstanding the anticipated improvements in OCT and even the present ability to reliably perform laser field designs for certain "simple" chemical applications,[73] it is reasonable to categorically state that, in the foreseeable future, closed-loop OCE will form the only practical means of achieving successful control of complex polyatomic molecules, especially with multiple product channels. Thus, section IIIC will express the general principles and procedures for closed-loop OCE.

B. Optimal Control Theory. A fundamental question to ponder before considering any control field design algorithms is whether any field exists that may lead to successful control in a particular quantum system. This question is addressed by a controllability analysis. Controllability tools are available to assess whether it is, in principle, possible to arbitrarily steer about the wave function[90] and the more general time evolution operator[91] in any given quantum system expressed in a finite dimensional basis. Although an affirmative answer to controllability of the wave function would immediately imply the

ability to control any physical observable for the system, the control of a particular observable should be a less demanding task to assess and possibly achieve. Even a respectable level of partial controllability may be quite adequate for many applications. However, the tools have yet to be developed for assessing controllability of arbitrary physical observables.

Putting aside fundamental issues of controllability, OCT forms a reliable design procedure to identify the best control field possible under a given set of conditions.[70,72,73,85,86] The most comprehensive means for controlling a molecule undergoing complex dynamical evolution is through coordination of the controlling electromagnetic field with the molecule's characteristics. The spectral content and temporal structure of the control field should be continuously alterable throughout the process. This tight coordination ensures that all of the dynamical capabilities (i.e., both electronic and nuclear) of the molecule can be exploited to best meet the chemical objectives. Given specified initial and final states of the molecule, as in eq 2, and any imposed restrictions on the field or molecular dynamics, the time-dependent control field required to meet the objective may be designed using OCT. This general formulation encompasses both the weak and strong field limits, and, in principle, is capable of discovering control methods based on two-pathway interference induced by monochromatic laser fields,[92,93] the "pump-dump" techniques based on two ultrashort laser pulses,[94,95] and control via stimulated Raman adiabatic passage.[96,97]

Optimal control theory has an extensive history in traditional engineering applications,[98] but the quantum nature of molecular-scale phenomena imposes special features. Consider a quantum system (e.g., a molecule), whose free evolution is governed by the Hamiltonian H_0. The full Hamiltonian of the laser-driven system is $H = H_0 - \mu\epsilon(t)$, with the dynamics prescribed by eq 3. A more complete picture with all electrons and nuclei specifically treated could be considered based on the Hamiltonian in eq 4. The goal of OCT is to design an electric field that will allow manipulation of the system dynamics in a desired way, subject to eq 3 being satisfied.

A typical quantum control objective is to maximize the magnitude of the expectation value $\langle\psi(T)|O|\psi(T)\rangle$ of a specified observable operator O at the final time T. For example, O might be the flux operator associated with a reactive channel, with the control objective being maximization of the product yield in that channel. In practice, there may be multiple objectives involving distinct observable operators corresponding to the desire to simultaneously manipulate several physical aspects of the same system (e.g., control the fate of multiple bonds in a polyatomic molecule). In addition, there may be costs or constraints on the form, magnitude, frequency, or other characteristics of the control field. These various objectives and constraints will often be in competition with each other. This recognition motivates posing the control design problem as an optimization attempting to strike a balance between the competing physical goals. Balancing such competition is an essential feature of OCT. The physical objectives are expressed collectively in a cost functional $J[\psi(t),\epsilon(t)]$, dependent on the evolving wave function[70] (or density matrix,[99] if appropriate), the target states or expectation values, any constraints, and the electric field. Physical input, often guided by intuition, will enter through the form and relative weight given to the different terms in the cost functional. The cost functional J is optimized with respect to the control field $\epsilon(t)$, to yield the best possible control performance in balance with any other competing factors.

Consider, for example, the case of maximizing the expectation value $\langle\psi(T)|O|\psi(T)\rangle$ of a positive definite operator O at the target time T, while minimizing the laser field fluence. In this circumstance, the cost functional may take the form

$$J = \langle\psi(T)|O|\psi(T)\rangle - \alpha_0\int_0^T [\epsilon(t)]^2\,dt - 2\Re\int_0^T \langle\chi(t)|i\hbar\partial_t - H|\psi(t)\rangle\,dt] \quad (14)$$

Here, $\partial_t = \partial/\partial t$,$\alpha_0$ is a positive parameter chosen to weight the significance of the laser fluence, $|\psi(t)\rangle$ is the system wave function, and $|\chi(t)\rangle$ is a Lagrange multiplier introduced to ensure satisfaction of the Schrödinger equation in the design process. Requiring that the first variation of J with respect to $|\psi(t)\rangle$, $|\chi(t)\rangle$, and $\epsilon(t)$ satisfy $\delta J = 0$ will give equations for the wave function, Lagrange multiplier, and optimized laser field:[70,72]

$$i\hbar\partial_t|\psi(t)\rangle = H|\psi(t)\rangle,|\psi(\mathbf{0})\rangle = |\psi_0\rangle \quad (15)$$

$$i\hbar\partial_t|\chi(t)\rangle = H|\chi(t)\rangle,|\chi(T)\rangle = O|\psi(T)\rangle \quad (16)$$

$$\epsilon(t) = -\Re\langle\chi(t)|\mu|\psi(t)\rangle/\alpha_0 \quad (17)$$

Here, $|\psi_0\rangle$ is the initial state of the quantum system. Numerical solution of the above equations will give the desired optimal control field, although this often is a problem of significant computational complexity. Specifically, the accurate solution of the many-dimensional Schrödinger equation in eqs 15 and 16 poses a significant challenge even for cases with a few atoms. Equations 15−17 will generally have multiple solutions corresponding to a family of locally optimal control field designs.[100] Various iterative algorithms have been developed for the calculation of optimal control fields and many numerical examples have demonstrated quantum optimal control of molecular-scale phenomena, (e.g., rotational, [101] vibrational,[102] electronic,[103] reactive,[104,105] and other processes.[106] In addition to achieving a balance among the physical objectives, the OCT design process may also include the goal of achieving the objectives while simultaneously having the process be as robust as possible to laser field errors or Hamiltonian uncertainties.[107]

The many OCT simulations performed in recent years have produced physical insight into the control of quantum phenomena. However, all of these efforts have been carried out with relatively simple systems or simple models of complex systems. Notwithstanding this comment, the most important result coming from the various OCT simulations is that successful control fields exist, capable of providing high quality molecular manipulation to meet many physical objectives. The significance of this conclusion stands, regardless of the fact that it is drawn from models of molecules and other systems. The ability to perform OCT will surely improve in the coming years, and it should continue to provide at least physical insight into virtually all control applications.

C. Optimal Control Experiments. Optimal control theory has proved to be a valuable theoretical tool for exploring coherent laser manipulation of quantum systems. However, attaining laboratory-significant OCT field designs requires precise knowledge of the system Hamiltonian, which often is not available for the most interesting molecules or materials, even for those of modest complexity. The quality of laser field designs is also limited by the ability to accurately solve the design equations. To appreciate the significance of these comments, recall that quantum control relies on the often delicate manipulation of matter wave interferences through the proper tuning of laser phases and amplitudes. It is reasonable to expect that there will be only limited tolerance to inevitable field design errors.

A crucial step toward attaining high-quality laboratory laser control of molecular-scale phenomena was the introduction of adaptive control techniques, initially suggested by Rabitz and Shi in 1991,[87] and elaborated on by Judson and Rabitz in 1992[2] and in subsequent investigation.[74−76,78−81] In this OCE approach, known as learning control, a loop is closed in the laboratory around the quantum system, with results of the control field → observable outcomes used to evaluate the success of the candidate applied laser field designs and to refine them, until the control objective is reached as best as possible with an optimal field. In learning control, a new molecular sample is used in each cycle of the loop, which (i) circumvents the possibly disruptive back action exerted by the measurement process on a quantum system, and (ii) permits the loop closure to be performed on laboratory apparatus cycling time scales (e.g., $\sim 10^{-3}$ s for liquid crystal laser modulators). The OCE learning process is based on the following realizations: (A) The molecule "knows" its own Hamiltonian, with no uncertainty. (B) When exposed to a laboratory control field, a molecule will solve its Schrödinger equation on ultrafast real molecular time scales, with absolute fidelity. (C) Laser pulse shapers with duty cycles of up to 10^4 distinct pulses per second are becoming available under full computer control. (D) Many physical objectives correspond to easily detectable outcomes, calling for little or no refined data analysis. (E) Fast algorithms exist to recognize patterns in the emerging control field → observable relationships, to automatically suggest new (better) control fields.

The synthesis of steps (A),...,(E) produces an efficient closed-loop learning procedure for teaching lasers to control quantum systems, and a schematic of this process is shown in Figure (2).

The learning control procedure for manipulating quantum systems generally involves five basic elements: (1) an input trial control laser design, (2) the laboratory apparatus for generation of shaped laser pulses, (3) application of the laser control fields to the quantum system sample, (4) observation of the resultant control outcome, and (5) a learning algorithm that analyzes the measurement results from the prior experiments and suggests a new control field to be used in the next loop cycle. All of the current closed-loop learning control experiments[1,30−32,35,88,89] were started by generating random initial control fields (i.e., side-stepping element (1) above). However, an OCT design may yield a good initial estimate for further laboratory OCE refinement as well as provide helpful guidance on the physical mechanism involved.[73,87]

An important enabling technology for laboratory quantum learning control is the ability to shape ultrafast laser pulses on the femtosecond scale.[108] This technology is presently available and rapidly improving. Phase and amplitude modulation of the frequency components of the dispersed pulse is performed in the focal plane typically by an acousto-optic modulator (AOM)[17] or by a liquid crystal modulator (LCM).[20] The advantages of the AOM include high spectral resolution and fast response time, but it suffers from low light transmission (typically, about 5%). A LCM exhibits high light transmission (about 80%) and easy implementation (these devices are commercially available for the spectral range from 430 nm to 1.6 μm). However, a LCM has low spectral resolution (typically 128 discrete pixels) and slow transformation times, requiring at least a millisecond to change the pixels. Fast transformation times are important for closed-loop learning control, which may require exploring many thousands of distinct pulse shapes before finding an optimal result. However, current molecular implementations are not significantly limited by the number of LCM pixels or the pixel transformation time.

The present pulse-shaping technology in the visible and near-infrared spectral ranges is suitable for exciting transitions between molecular electronic surfaces and for the manipulation of highly excited molecular vibrations. Further progress in the development of pulse shapers working in the mid- and far-infrared spectral ranges is necessary for control of molecules in their ground electronic state. The stability of pulse shapers appears to be adequate for the majority of chemical applications. The presence of modest noise in the laser electric field does not limit the quality of laboratory learning techniques employing evolutionary algorithms, and can even help the search for a better solution in a complex multidimensional parameter space.[74,75,80] The opinion existed just a few years ago that the use of monochromatic lasers for control would be preferable in practice because laboratory learning control with tailored pulses would be too difficult to implement. However, recent advances in pulse-shaping technology have made this point of view obsolete, as demonstrated by closed-loop laboratory methods employing ultrashort shaped laser pulses that are rapidly becoming common experimental practice, with excellent reliability.

There is no need to measure the laser field in the learning process, because any systematic characterization of the control "knobs" (e.g., pulse shaper parameters) is sufficient. This set of control knobs, determined by the experimental apparatus, defines the parameter space to be searched by the learning algorithm for an optimal laser shape. The closed-loop OCE procedure naturally incorporates any laboratory constraints on the control laser fields. Moreover, the algorithm will identify only those pathways to desired products that are adequately robust to inevitable random disturbances encountered in the laboratory.[80]

The learning algorithm should be sufficiently intelligent to ensure that the cyclic control process will converge on the objective. A variety of learning algorithms may be employed,[75,76,79] but following the original proposal,[2] the recent laboratory studies[1,31−33,35,84,88,109−111] have focused on the use of evolutionary genetic algorithms[26,112−114] as global search techniques. These techniques are quite effective even when noise is present,[74,75,80] both in the measurements of the control outcome and in the tuning of the laser field.

In contrast to excellent OCE performance, global search techniques are very difficult to use in numerical OCT simulations of learning control, because they demand enormous computational efforts.[112] In such theoretical simulations, the global search for the optimum requires numerous iterations of the computationally intensive task of solving the time-dependent Schrödinger equation. However, in OCE learning control, the global search is remarkably efficient, because the evolving quantum system naturally "solves" its Schrödinger equation as accurately and as fast as possible. This OCE procedure eliminates the numerical burden of solving Schrödinger's equation and allows for real-time adaptive control in the closed-loop experiments.

Although algorithms of the evolutionary type (e.g., genetic algorithms) are technically effective, they suffer from the conceptual drawback that little information about the control mechanisms is gained from the optimum search process. Recent progress has been made toward designing new algorithms for laboratory control that bring more insight into the physical processes operative in the controlled system.[81] One approach uses high-dimensional model representation (HDMR), which provides a systematic means to experimentally determine the

functional relationship between the applied control field and the resulting value of the control objective.[115,116] In HDMR, the input (e.g., the control field) and the output (e.g., the control objective) are related through a hierarchy of control variable correlations. Nonlinear input → output maps based on HDMR have been recently employed to create an algorithm for laboratory learning control.[81] This task is facilitated by expressing the control phases, amplitudes, or other laboratory parameters as a set of n input variables $(x_1,...,x_n) \equiv x$. A hierarchical map between a laboratory observable O and x may be written as

$$O(x) = O_0 + \sum_i O_i(x_i) + \sum_{i<j} O_{ij}(x_i,x_j) + ... \qquad (18)$$

Here, O_0 is the constant mean response, $O_i(x_i)$ describes the independent action of variable x_i, and $O_{ij}(x_i,x_j)$ describes the cooperative effect of the variables x_i,x_j, etc. Within HDMR, an input → output map (i.e., the significant functions on the right-hand side of eq 18) is learned from laboratory data and may be used to facilitate the search for the optimal control field. An important feature of this algorithm is that the HDMR maps reveal the degree to which each field variable contributes to the desired control output, as well as the relative importance of correlations (e.g., O_{ij}) between different field parameters. The analysis of this information can be valuable even if the HDMR maps are not used for optimization, as they can clarify the physical mechanisms of control over molecular-scale processes.

Short of performing additional observations of the evolving controlled molecule, the primary clues about quantum control mechanisms are contained in the available control field. But before any reliable physical analysis of the field can be made, it is first necessary to ensure that the control field contains only those features that are truly required to achieve the control objective. Such a field cleanup must be done while the OCE learning process is being executed in the laboratory. An algorithm for this purpose was recently introduced and demonstrated in simulations.[80] It should be readily implemented in the laboratory, as it calls for no basic change in the OCE hardware.

In summary, closed-loop learning algorithms provide a broad generic tool for teaching a laser how to manipulate quantum phenomena of any type. The technique may operate with any suitable laser and detector appropriate for the particular physical system and its chosen objectives. As shown in the next section, closed-loop OCE in the strong field regime is especially attractive, as it can form a generic means for manipulating molecules and other quantum systems.

IV. Strong Field Control Using Tailored Laser Pulses

A. Experimental. To implement the OCE closed-loop control paradigm in the strong field regime three technologies are combined: (1) regenerative amplification of ultrashort pulses; (2) pulse shaping using spatial light modulation; and (3) some feedback detection system, (i.e., time-of-flight mass spectral detection in the experiments presented here). An overview of this implementation of the closed-loop control experiment is shown in Figure 11. Briefly, the experiment begins with a computer generating a series of random, time-dependent laser fields (40 such control pulses are employed in the experiments presented here). In some cases, prior estimates for fields might be available by design or from related systems to introduce specific trial field forms. Each of the control pulses is amplified into the strong field regime and subsequently interacts with the gas phase sample under investigation. Products are measured

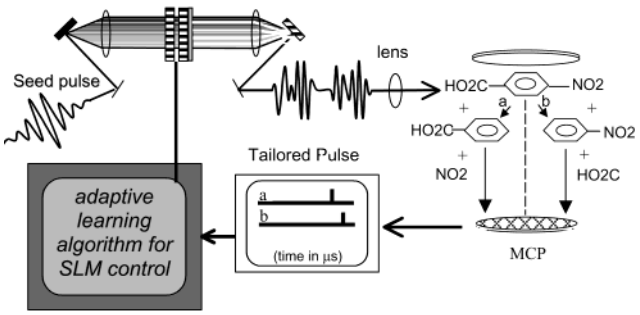

Figure 11. Schematic of the closed-loop apparatus for tailoring the time-dependent laser fields to produce the desired reaction product. In this scheme an algorithm controls the spatial light modulator that produces a well-defined waveform. The tailored light pulse interacts with the molecular sample to produce a particular product distribution. The product distribution is rapidly measured using time-of-flight mass spectrometry and the results are fed back into the control algorithm. The same closed-loop concept with other sources or detectors can be applied to control a broad variety of quantum phenomena.

using time-of-flight mass spectrometry, and this requires approximately 10 μs to detect all of the ion fragments. The mass spectra are signal averaged with a number of repeats for the same pulse shape and analyzed by the computer to determine the quality of the match to the desired goal. The remainder of the control fields sequentially interact with the sample, and the fitness of the products are also stored on a computer. After each of the 40 control fields have been analyzed in terms of the product distribution, the results of the fitness are employed to determine which fields will be used to create the next set of laser pulses for interaction with the sample. The system iterates until an acceptable product distribution has been achieved.

The technique of regenerative amplification will be briefly described to better understand the pulse shaping method for implementing the control strategy. Kerr lens mode locking in an Ar ion-pumped Ti:sapphire crystal is used to generate the initial short pulse. With our system the pulse duration is approximately 20 fs and is supported in 80 nm of bandwidth centered at 800 nm. The production of the short pulse occurs when the frequencies of the emission of the Ti:sapphire are phase locked according to

$$\sum_i \cos(\omega_i t + \phi_i) \qquad (19)$$

where the relative phase, ϕ_i, is zero for each of the frequency components. Before amplification can occur, the pulse must be stretched from 20 fs to approximately 100 ps so that damage of the optics does not occur. Stretching is accomplished by making each frequency travel a different, well-defined path length before amplification. This is accomplished in our system by first dispersing the radiation using a grating as shown in Figure 12. The radiation is then collimated using a lens and is refocused onto a second grating. If the second grating is at the focal point of the second lens, no stretching occurs to the radiation and such an optical layout is termed a zero length stretcher. This stretching configuration is used (without retroreflection) in spatial light modulation schemes. If the second grating is not at the focal point of the second lens, the redder frequencies of the radiation travel a shorter path length than the blue frequencies and the pulse is stretched to a desired duration that depends on the path length difference. Most importantly, the relative phase delay between the frequency components can be compensated for after amplification in a second optical device, the compressor.

After stretching, the pulse amplification occurs in a second Ti:sapphire cavity that is pumped by a Nd:YAG laser. The pulse

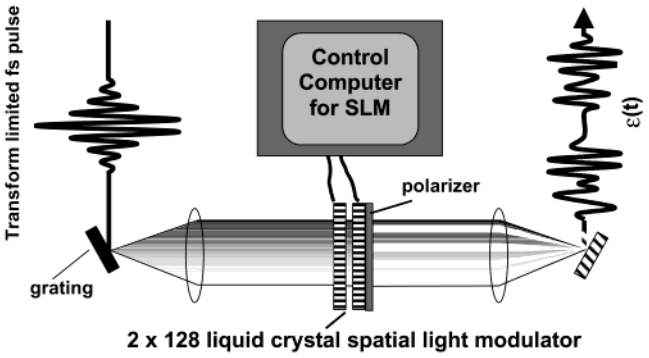

Figure 12. Schematic of the optical setup for generating a shaped laser pulse. See text for description of the optical elements.

is amplified by passage through the gain medium on the order of 15 times, and the amplified pulse is fed to a dual grating compressor to return the relative phase of the frequency components as close as possible to the initial values. The distance between the grating pair can be adjusted to compensate for second order retardation effects of the optical components and thus minimize the duration of the amplified pulse. At a grating separation greater (less) than the optimal setting, the bluer (redder) frequencies lead the redder (bluer) frequencies producing a so-called negatively (positively) chirped pulse. The pulse duration can be adjusted using the separation in the gratings or by altering the bandwidth of the laser pulse that is amplified. Less bandwidth leads to longer pulse duration. Regenerative amplifiers have an intrinsic bandwidth limit due to gain narrowing, a phenomenon that arises because the laser gain profile is not a uniform function of frequency. There is a preferred frequency (having the highest gain) that becomes amplified at the expense of frequencies having lower gain.

To shape the laser pulse we first transform the pulse into frequency space using a zero length stretcher. The apparatus for this is shown in Figure 12. In the plane between the two lenses of the stretcher (the so-called Fourier plane) each of the frequency components of the pulse can be spatially addressed with high resolution. Modification of the relative phases and amplitudes of these components will change the shape of the time-dependent laser electric field after recombination on the second grating. To modify the phase and amplitude of the dispersed frequency components a CRI liquid crystal spatial light modulator is employed. This device has two arrays of liquid crystals, each having 128 pixels that are 100 μm wide and 2 mm high. The dead space between pixels is 3 μm. The arrays have crossed polarization axes. When followed by a polarization element, the sum of the retardances provides the phase modulation, ϕ_i, and the difference of the retardances provides the amplitude modulation. The retardance is set by specifying a voltage (between 0 and 10 V with 8-bit resolution in our case) to be applied to the liquid crystal. The set of the 2×128 voltages uniquely specifies the time-dependent electric field.

The voltages used to specify a time-dependent electric field are determined on the fly upon each cycle of the closed-loop by the computer using a genetic algorithm. The genetic algorithm produces a set of 40 time-dependent electric fields using the methods of cloning, crossover, and mutation. When cloned, the electric field with the best fitness value is simply copied *n* number of times in the next generation. A cloning rate of 2 provided good convergence rates in these experiments. Crossover denotes an operator that allows exchange between two tailored pulses. In this process two voltage arrays (genomes), A and B, are copied verbatim up to a randomly chosen element in the arrays. After that point the remaining genome of A is switched with B, while the remainder of B is switched with A. Mutation refers to a process where each voltage in the new genome has some probability to be modified to a new random value. For these experiments a mutation rate of 6% per pixel was found to acceptable convergence rates. The particular rates of mutation and crossover are specific to each laser system, detection scheme, and physical system.

B. Trivial Control of Photochemical Ion Distributions. We first consider whether manipulation of the dissociation distribution can be achieved by simple alteration of either pulse energy or pulse duration. These are termed trivial control methods, and in either case there is no need to systematically manipulate the relative phases of the constituent frequency components. Pulse energy modulation is achieved here using a combination of a polarization rotator and beam splitter or by the use of thin glass cover slips to reflect away several percent of the beam. Pulse duration control can be implemented by either restricting the bandwidth of the seed laser or by placing a chirp onto the amplified pulse in the compressor optics.

Investigations of trivial control suggest that the ionization/fragmentation distribution can often be manipulated by altering either pulse energy or pulse duration. Whether this is a general observation for all molecular systems is under active investigation. As an example, Figure 13 shows the mass spectral distributions measured for *p*-nitroanaline as a function of either pulse duration (Figure 13a) or pulse energy (Figure 13b). In the case of the transform limited mass spectrum at 10^{14} W cm^{-2}, there are many features in the mass spectrum corresponding to production of the $C_{1-5}H_x^+$ fragments. There is a minor peak at *m*/*e* 138 amu corresponding to formation of the parent molecular ion. We observe that when the pulse duration is increased the fragmentation distribution shifts toward lower mass fragments. This indicates an enhanced opportunity for ladder switching during the excitation process. Ladder switching allows facile excitation of the internal modes of the molecule.[9] Increasing the pulse duration also leads to lowering the pulse intensity. Alternatively, to lower the pulse intensity, the pulse energy can be reduced. When this form of trivial control is implemented, a completely different mass spectral distribution is obtained, as shown in Figure 13b. When the intensity is reduced by a factor of 5, the parent molecular ion becomes one of the largest features in the mass spectrum. These results suggest that in any control experiment a series of reference experiments probing the products as a function of pulse energy and duration are necessary to rule out the possibility of trivial effects.

C. Closed-loop Control of Selective Bond Cleavage Processes. Closed-loop control in the strong field regime has now been demonstrated on a series of ketone molecules.[1] We begin with acetone as a simple polyatomic system. Figure 14 displays the transform limited mass spectrum resulting from the interaction of acetone vapor with a pulse of duration 80 fs and intensity 10^{13} W cm^{-2}. There are a number of mass spectral peaks corresponding to various photoreaction channels as summarized in Scheme 1. Channel (a) corresponds to simple removal of an electron from the molecule to produce the intact acetone radical cation at $m/e = 58$. As noted in the Introduction, the ability to observe the intact molecule in the mass spectrum reveals that not all of the excitation energy necessarily couples into nuclear modes. The second pathway, (b), observed is cleavage of one methyl group to produce the CH_3CO and methyl ions. The third pathway corresponds to the removal of two methyl species to produce the CO and methyl ions. Only one of the product species in each channel is shown with a positive charge. Clearly there will be a probability for each of the product species to be

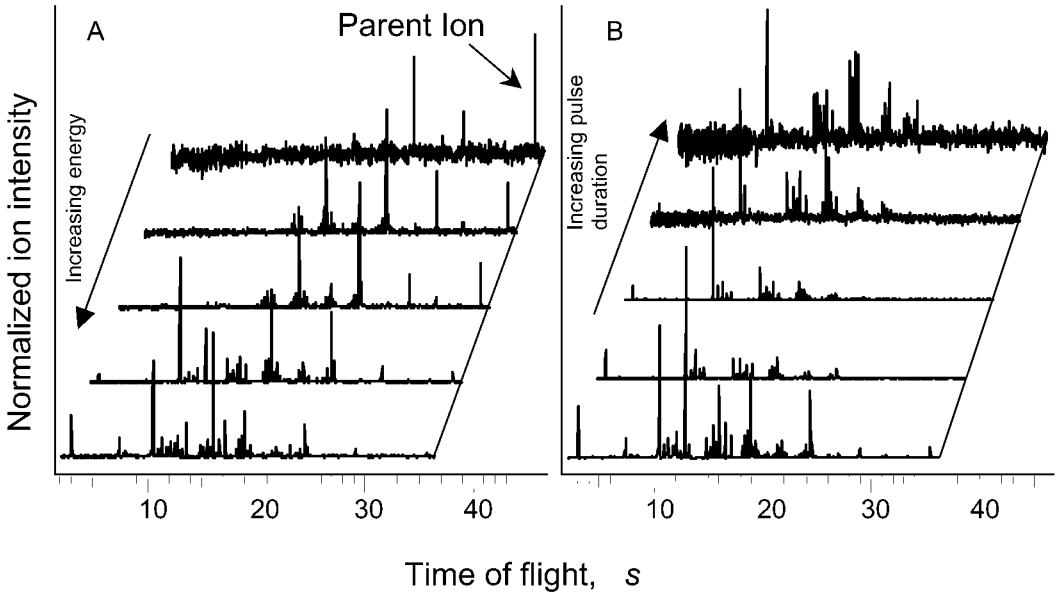

Figure 13. Time-of-flight ion spectra of *p*-nitroaniline after excitation using pulses centered at 790 nm, of duration 80 fs. In panel a the pulse energy was varied from 0.60 to 0.10 mJ/pulse, the pulse duration was 80 fs. In panel b the pulse duration was varied from 100 fs to 5 ps, the pulse energy was 0.60 mJ/pulse.

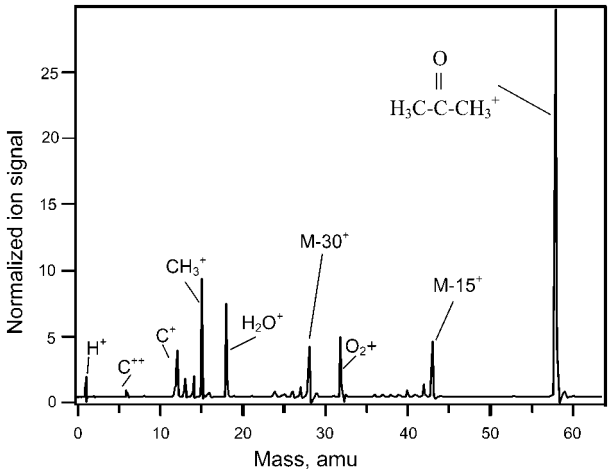

Figure 14. Time-of-flight mass spectrum for acetone after excitation using 5×10^{13} W cm^{-2}, 800 nm radiation of duration 60 fs. The prominent peaks in the mass spectrum are marked.

SCHEME 1

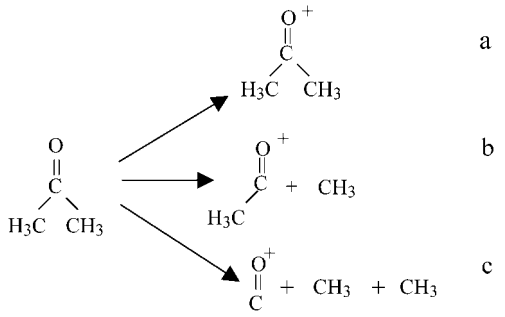

ionized that depends on the details of the laser pulse, the fragment's electronic and nuclear structure, and the dissociation pathway.

One of the simplest illustrations of the OCE closed-loop control algorithm is the case of enhancing the CH_3CO ion signal from acetone. This corresponds to specifying optimization of the second pathway b shown in Scheme 1. Using this criterion, representative mass spectra are shown as a function of generation

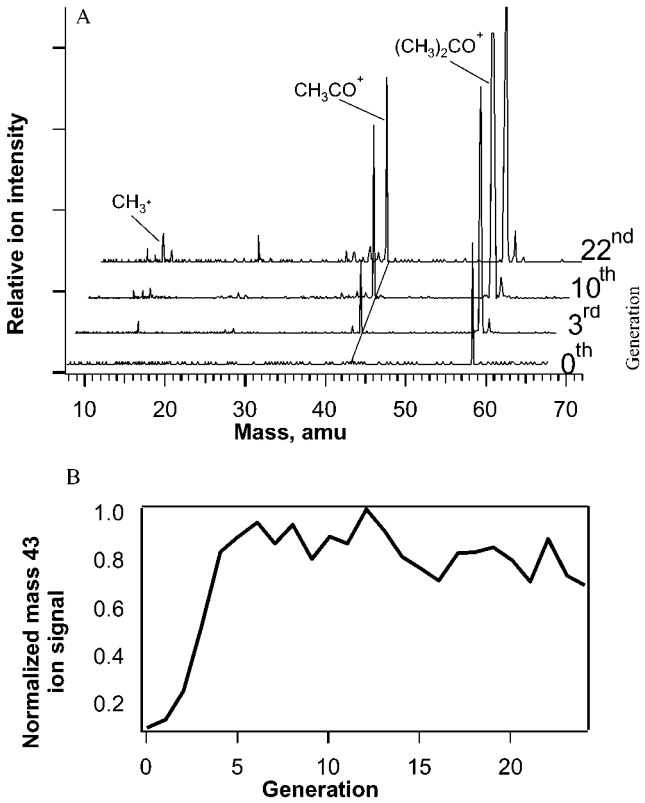

Figure 15. (A) Representative mass spectra of acetone ($CH_3-CO-CH_3$) for the initial 0th, 3rd, 10th, and 22nd generations of the laboratory learning process when maximization of the CH_3CO^+ ion from acetone is specified. (B) CH_3CO^+ signal as a function of generation of the genetic algorithm. In (B) and the following plots of this type, the average signal for the members of the population at each generation is shown.

in Figure 15 when the algorithm has been directed to increase the intensity of the methyl carbonyl ion at $m/e^- = 43$ amu. The intensity of this ion increases by an order of magnitude by the fifth generation in comparison with the initial randomly generated pulses and is seen to saturate shortly thereafter. The modulation in the signal in subsequent generations is largely

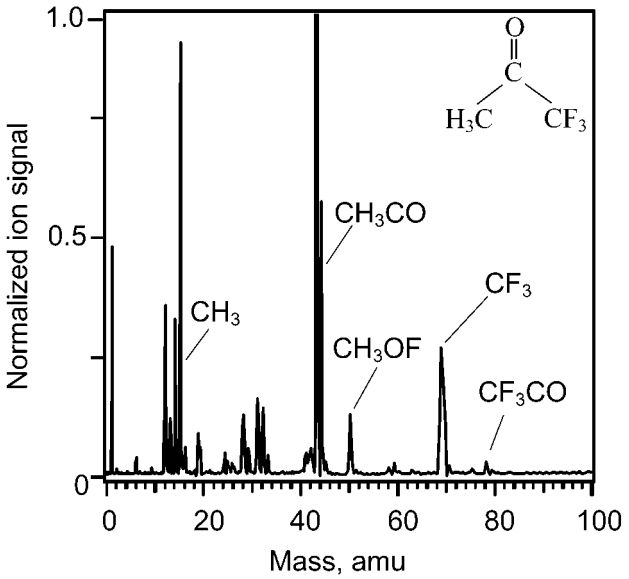

Figure 16. Time-of-flight mass spectrum for trifluoroacetone ($CF_3-CO-CH_3$) after excitation using 5×10^{13} W cm^{-2}, 800 nm radiation of duration 60 fs. The prominent peaks in the mass spectrum are marked.

SCHEME 2

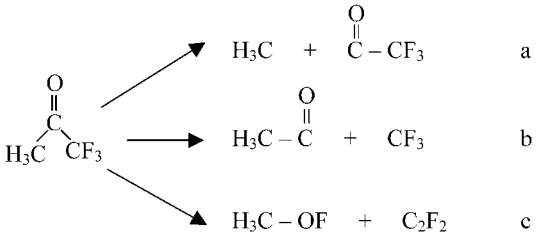

due to the algorithm searching new regions of amplitude and phase control field space through the operations of mutation and crossover. The experiment demonstrated two important features of the closed-loop control. The first was that the algorithm was capable of finding suitable solutions in a reasonable amount of laboratory time (10 min in this case). The second was that the shaped strong field pulses were able to dramatically alter the relative ion yields and thus the information content in a mass spectrum. We anticipate that the method will have important uses as an analytical tool based on this capability. Finally, the control exerted in this case is of the trivial form, and is due to intensity control as indicated by the masks showing that the optimal pulse was near transform limited and of full intensity. The reference experiments also demonstrated that intense transform limited pulses resulted in a similar fragmentation distribution.

The control over the selective cleavage of various functional groups has been investigated using the molecules trifluoroacetone and acetophenone. Trifluoroacetone was investigated because there are two distinct unimolecular decomposition routes as shown in Scheme 2 a and b.

Figure 16 displays the mass spectrum associated with the transform limited, intense laser excitation of trifluoroacetone. The ions of importance in the spectrum include peaks at *m*/*e* 15, 28, 43, 69, and 87 corresponding to CH_3, CO, CH_3CO, CF_3, and CF_3CO. These peaks are associated with cleavage of the methyl, fluoryl, or both species from the carbonyl group as indicated in Scheme 2. Interestingly, there is also a feature at *m*/*e* = 50 amu that can only be assigned to CH_3OF shown in pathway (c). This species must be formed by an intense field

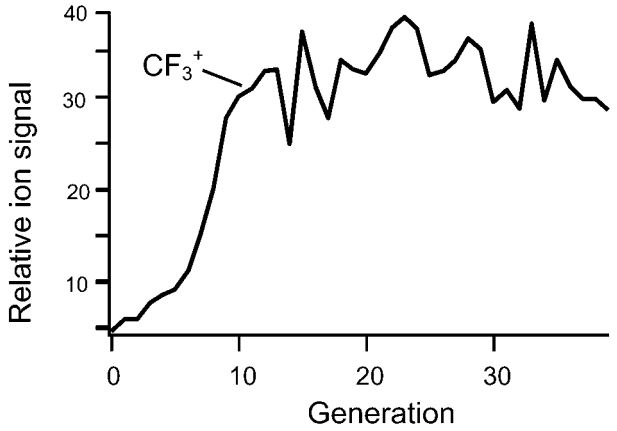

Figure 17. CF_3+ signal as a function of generation of the genetic algorithm. In this experiment the cost functional was designed to simply optimize this signal.

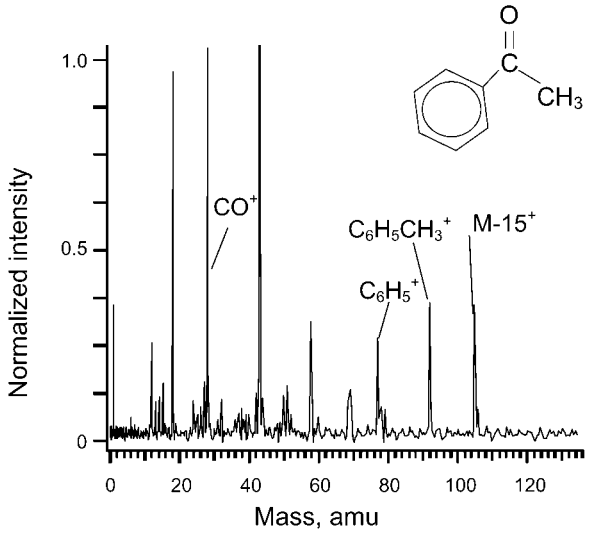

Figure 18. Time-of-flight mass spectrum for acetophenone ($C_6H_5-CO-CH_3$) after excitation using 5×10^{13} W cm^{-2}, 800 nm radiation of duration 60 fs. The prominent peaks in the mass spectrum are marked.

rearrangement process and has not been observed in the weak field regime of photochemical reactivity. Such rearrangement processes are discussed in more detail in section IV.4.

The ability of the closed-loop control to cleave a specific bond is demonstrated in Figure 17 where we have specified that the algorithm search for solutions enhancing the signal at *m*/*e* = 59. This ion corresponds to the CF_3 species. Figure 17 demonstrates that the closed-loop OCE method may be used to enhance the desired ion signal by a factor of approximately 30 in comparison with the initial random pulses. While this experiment was successful in enhancing the desired ion yield, it does not necessarily demonstrate control. Control is achieved when one channel is enhanced at the expense of another.

To demonstrate control over selective cleavage of specified bonds in a molecule we consider acetophenone, a system that has a carbonyl species bound to methyl and phenyl functional groups. The transform limited mass spectrum for acetophenone is shown in Figure 18. There are numerous peaks detected in the spectrum revealing that there are a multitude of decomposition paths available after excitation. The ions observed at 15 and 105 amu correspond to the species obtained after cleavage of the methyl group. The pair of ions at 77 and 43 amu correspond to cleavage of the phenyl group. The dissociation

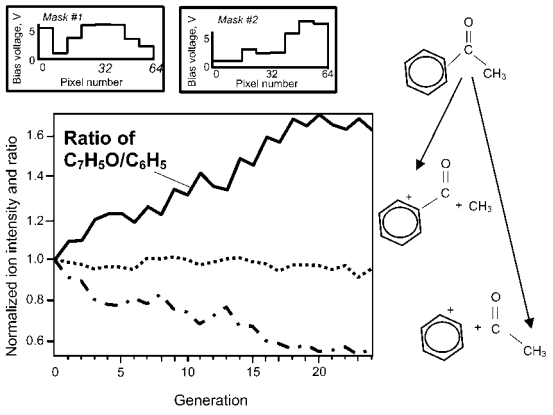

Figure 19. Relative ion yield for phenylcarbonyl (dotted) and phenyl (dashed) and the $C_6H_5CO^+/C_6H_5+$ ratio (solid) as a function of generation when maximization of this ratio is the specified goal in the closed-loop experiment. The optimal masks resulting from the closed-loop process are shown in the inset.

SCHEME 3

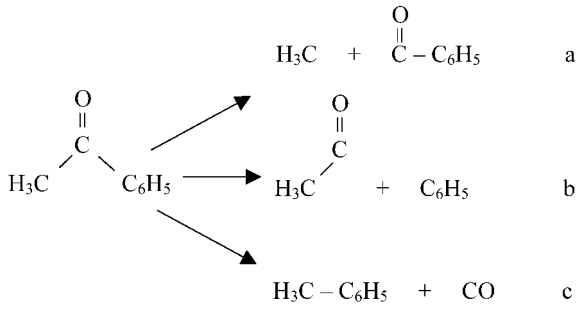

and rearrangement reactions investigated for this molecule are shown in Scheme 3.

Scheme 3(c) implies the rearrangement of acetophenone to produce toluene and CO, and this is signified in the mass spectrum by peaks at 92 and 28 amu, respectively. To determine whether a path can be selectively enhanced, we specified enhancement of the ion ratio for the species C_6H_5CO/C_6H_5. This denotes selective cleavage of the methyl group at the expense of the phenyl group. Note that we do not stipulate how the ratio should be increased, i.e., increase C_6H_5CO or decrease C_6H_5. Picking a particular path could be done with another cost functional. The ratio as a function of generation is shown in Figure 19. The ratio increases by approximately a factor of 2 after 20 generations. Other ions could have been chosen to control the cleavage reaction, the two chosen happen to be experimentally convenient. Thermodynamically, the goal of enhancing methyl dissociation is the favored cleavage reaction because the bond strength of the methyl group is 15 kcal less than that of the phenyl group.[117] The ratio of phenyl ion to phenyl carbonyl can also be enhanced as shown in Figure 20. The learning curve for this experiment reveals that the phenyl carbonyl ion remains relatively constant while the phenyl ion intensity increases. This is interesting because the energy required to cleave the phenyl-CO bond is 100 kcal while the methyl-CO bond requires 85 kcal. Thus the ratio of these ions can be controlled over a dynamic range of approximately five in the previously reported experiment[1] and a dynamic range of up to 8 has been recently observed.

The goal of laser control of chemical reactivity transcends the simple unimolecular dissociation reactions observed to date.[1,32−34,37] Observation of the toluene ion in the strong-field acetophenone mass spectrum suggests that control of molecular dissociative rearrangement may be possible. To test this

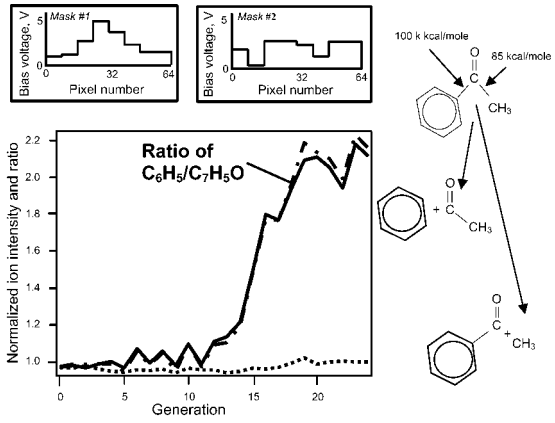

Figure 20. Relative ion yield for phenylcarbonyl (dotted) and phenyl (dashed) and the $C_6H_5+/C_6H_5CO^+$ ratio (solid) as a function of generation when maximization of this ratio is specified. The optimal masks resulting from the closed-loop process are shown in the inset.

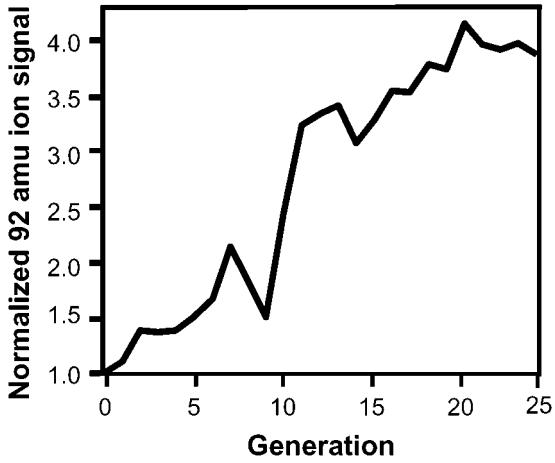

Figure 21. Average signal for toluene, 92 amu, as a function of generation when maximization of the ion signal for this reaction product was specified for optimization. Corresponding electron-impact-ionization mass spectrometry revealed no evidence for toluene in the sample.

SCHEME 4

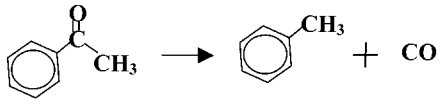

hypothesis we specified the goal of maximizing the toluene yield from acetophenone, as shown in Scheme 4. For toluene to be produced from acetophenone, the loss of CO from the parent molecule must be accompanied by formation of a bond between the phenyl and methyl substituents. The closed-loop control procedure produced an increase in the ion yield at 92 amu of a factor of 4 as a function of generation as shown in Figure 21. As a further test, we specified maximization of the ratio of toluene to phenyl ion and observed a similar learning curve to that in Figure 20; with an enhancement in the toluene-to-phenyl ratio of a factor of 3. Again, the final tailored pulse does not resemble the transform-limited pulse. To confirm the identity of the toluene product, measurements on the deuterated acetophenone molecule $C_6H_5COCD_3$ were carried out and the $C_6H_5CD_3^+$ ion was the observed product in an experiment analogous to Figure 21. The observation of optically driven dissociative rearrangement represents a new capability for strong field chemistry. In fact conventional electron-impact mass spectrometric analysis of acetophenone is incapable of creating

toluene in the cracking pattern. In strong-field excitation, the molecular electronic dynamics during the pulse is known to be extreme, and substantial disturbance of the molecular eigenstates (compare with Figure 1) can produce photochemical products, such as novel organic radicals, that are not evident in the weak-field excitation regime. Operating in the strong field domain opens up the possibility of selectively attaining many new classes of photochemical reaction products.

Extensive manipulation of mass spectra is possible when shaped, strong field laser pulses interact with molecules under closed-loop control. The control pulses occur with intensity of $\sim 10^{13}$ W cm^{-2} where the radiation significantly disturbs the field-free eigenstates of the molecule. Even in this highly nonlinear regime, the learning algorithm can identify pulse shapes that selectively cleave and rearrange organic functionality in polyatomic molecules. These collective results suggest that closed-loop strong field laser control may have broad applicability in manipulating molecular reactivity. The relative ease in proceeding from one parent molecule to another should facilitate the rapid exploration of this capability.[1]

The limit on the range in control in the examples shown here may be due to a number of factors. The first is that we have employed a limited search space by ganging a series of eight collective pixels in each of the two masks to produce a total of 16 variable elements. We have observed that relaxing this restriction leads to a much longer convergence time, and while a better result is expected, we have not observed such to date. However, other researchers have employed schemes using all pixels, as well as schemes to constrain the amplitude and phase search space.[26,113] Furthermore, the mass spectrometer was limited to eight averages for these experiments so that convergence can occur on a reasonable time scale. Obviously longer averaging will require longer experiment times. This parameter is under investigation at the present time. Another reason for limited dynamic range is the requirement that the same pulse used to alter the nuclear dynamics also must produce ionization. Each of these processes requires a different pulse time scale. In the case of ionization, the shortest pulse possible, ~10s of fs, is best for high ionization rates with little dissociation. For the control of the nuclear wave packet it is expected that a pulse with duration on the time scale of nuclear motion, ~ps, should be optimal. Thus, separation of these two processes should lead to a higher dynamic range.

V. Conclusion

Recent progress in the understanding of fundamental quantum control concepts and in closed-loop laboratory techniques opens the way for coherent laser control of a variety of physical and chemical phenomena. Ultrafast laser pulses, with shapes designed by learning algorithms, already have been used for laboratory control of many quantum processes, including unimolecular reactions in the gas and liquid phases, formation of atomic wave packets, second harmonic generation in nonlinear crystals, and high harmonic generation in atomic gases. One may expect a further increase in the breadth of controlled quantum phenomena, as success in one area should motivate developments in others. The various applications of coherent laser control, no matter how diverse, all rely on the same principal mechanism: the quantum dynamics of a system is directed by the tailored interference of wave amplitudes, induced by means of ultrafast laser pulses of appropriate shape. An important question is whether applications exist for which coherent laser control of molecular reactions offers special advantages (e.g., new products or better performance) over working in the traditional fully incoherent kinetic regime. Finding these applications will be of vital importance for the future progress of coherent control in chemistry and physics.

In addition to the practical utilization of laser control, the ultimate implications for controlling quantum processes may reside in the fundamental information extracted from the observations about the interactions of atoms. The following is intuitively clear: the more complete our knowledge of a quantum system, the better our ability to design and understand successful controls. But, is it possible to exchange the tools and the goals in this logical relationship and use control as a means for revealing more information on properties of microscopic systems? A challenging objective is to use observations of the controlled molecular dynamics to extract information on the underlying interatomic forces. Attaining precise knowledge of interatomic forces[73] has been a long-standing objective in the chemical sciences, and the extraction of this information from observed coherent dynamics requires finding the appropriate data inversion algorithms.

Traditionally, the data from various forms of continuous wave spectroscopy have been used in attempts to extract intramolecular potential information. Although such spectroscopic data are relatively easy to obtain, serious algorithmic problems have limited their inversion to primarily diatomic molecules or certain special cases of polyatomics. Analyses based on traditional spectroscopic techniques suffer from a number of serious difficulties, including the need to assign the spectral lines and to deal with inversion instabilities. An alternative approach to the inversion problem is to use an excited molecular wave packet that scouts out portions of the molecular potential surfaces. The sensitive information about the intramolecular potentials and dipoles may be read out in the time domain, either by probing the wave packet dynamics with ultrashort laser pulses or via measurements of the emitted fluorescence. A difficulty common to virtually all inverse problems is their ill-posedness (i.e., the instability of the solution against small changes of the data) which arises because the data used for the inversion are inevitably incomplete. Recent studies suggest that experiments in the time domain may provide the proper data to stabilize the inversion process.[118,119] In this process, the excitation of the molecular wave packet and its motion on a potential energy surface may be guided by ultrafast control laser fields. Control over the wave packet dynamics in this context can be used to maximize the information on the molecular interactions obtained from the measurements. The original suggestion[87] for using closed-loop techniques in quantum systems was for the purposes of gaining physical information about the system's Hamiltonian. Now that closed-loop OCE is proving to be a practical laboratory procedure, the time seems right to consider refocusing the algorithms and laboratory tools to reveal information on fundamental physical interactions.

Acknowledgment. The authors acknowledge the support of the Office of Naval Research, the Army Research Office, the National Science Foundation ,and the Sloan and Dreyfus foundations for the support of this research. R.J.L. acknowledges fruitful discussions with G. Menkir, A.N. Markevitch, N.P. Moore, and P. Graham and the assistance of B. Preutz with preparation of the manuscript.

References and Notes

(1) Levis, R. J.; Menkir, G. M.; Rabitz, H. *Science* **2001**, *292*, 709.
(2) Judson, R. S.; Rabitz, H. *Phys. Rev. Lett.* **1992**, *68*, 1500.
(3) Dewitt, M. J.; Levis, R. J. *J. Chem. Phys.* **1995**, *102*, 8670.
(4) L'Huillier, A.; Balcou, Ph. *Phys Rev. Lett* **1993**, *70*, 774.

(5) Agostini, P. F.; Fabre, F.; Mainfray, G.; Petite, G.; Rahman, N. K. *Phys Rev. Lett.* **1979**, *42*, 1127.
(6) Zavriyev, A.; Bucksbaum, P. H.; Squier, J.; Saline, F. *Phys. Rev. Lett.* **1993**, *70*, 1077.
(7) Kosmidis, C.; Tzallas, P.; Ledingham, K. W. D.; McCanny, T.; Singhal, R. P.; Taday, P. F.; Langley, A. J. *J.Phys. Chem. A* **1999**, *103*, 6950.
(8) DeWitt, M. J.; Peters, D. W.; Levis, R. J. *Chem. Phys.* **1997**, *218*, 211.
(9) Levis, R. J.; DeWitt, M. J. *J. Phys. Chem. A* **1999**, *103*, 6493.
(10) Villeneuve, D. M.; Aseyev, S. A.; Dietrich, P.; Spanner, M.; Ivanov, M. Y.; Corkum, P. B. *Phys. Rev. Lett.* **2000**, *85*, 542.
(11) Purnell, J. S., E. M.; Wei, S.; Castleman, A. W., Jr. *Chem. Phys. Lett.* **1994**, *229*, 333.
(12) Schmidt, M.; Normand, D.; Cornaggia, C. *Phys. Rev. A* **1994**, *50*, 5037.
(13) Ditmire, T.; Zweiback, J.; Yanovsky, V. P.; Cowan, T. E.; Hays, G.; Wharton, K. B. *Nature* **1999**, *398*, 489.
(14) Gavrilla, M. *Atoms in Intense Fields*, Academic Press: New York, 1992.
(15) Tannor, D. J.; Rice, S. A. *Adv. Chem. Phys.* **1988**, *70*, 441.
(16) Brumer, P.; Shapiro, M. *Laser Part. Beams* **1998**, *16*, 599.
(17) Warren, W. S.; Rabitz, H.; Dahleh, M. *Science* **1993**, *259*, 1581.
(18) Shapiro, M.; Brumer, P. Coherent control of atomic molecular, and electronic processes. In *Advances in Atomic Molecular and Optical Physics*, 2000; Vol. 42; p 287.
(19) Rabitz, H.; de Vivie-Riedle, R.; Motzkus, M.; Kompa, K. *Science* **2000**, *288*, 824.
(20) Weiner, A. M. *Optical Quantum Electron.* **2000**, *32*, 473.
(21) Tull, J. X. D., M. A.; Warren, W. S. *Adv. Magnetic Optical Reson.* **1996**, *20*.
(22) Yelin, D.; Meshulach, D.; Silberberg, Y. *Optics Lett.* **1997**, *22*, 1793.
(23) Brixner, T.; Oehrlein, A.; Strehle, M.; Gerber, G. *Appl. Phys. B* **2000**, *70*, S119.
(24) Efimov, A.; Moores, M. D.; Beach, N. M.; Krause, J. L.; Reitze, D. H. *Optics Lett.* **1998**, *23*, 1915.
(25) Uberna, R.; Amitay, Z.; Loomis, R. A.; Leone, S. R. *Faraday Discuss.* **1999**, 385.
(26) Hornung, T.; Meier, R.; Motzkus, M. *Chem. Phys. Lett.* **2000**, *326*, 445.
(27) Meshulach, D.; Silberberg, Y. *Nature* **1998**, *396*, 239.
(28) Hornung, T.; Meier, R.; Zeidler, D.; Kompa, K. L.; Proch, D.; Motzkus, M. *Appl. Phys. B* **2000**, *71*, 277.
(29) Weinacht, T. C.; Ahn, J.; Bucksbaum, P. H. *Nature* **1999**, *397*, 233.
(30) Bartels, R.; Backus, S.; Zeek, E.; Misoguti, L.; Vdovin, G.; Christov, I. P.; Murnane, M. M.; Kapteyn, H. C. *Nature* **2000**, *406*, 164.
(31) Bardeen, C. J.; Yakovlev, V. V.; Wilson, K. R.; Carpenter, S. D.; Weber, P. M.; Warren, W. S. *Chemical Physics Lett.* **1997**, *280*, 151.
(32) Assion, A.; Baumert, T.; Bergt, M.; Brixner, T.; Kiefer, B.; Seyfried, V.; Strehle, M.; Gerber, G. *Science* **1998**, *282*, 919.
(33) Vajda, S.; Bartelt, A.; Kaposta, E. C.; Leisner, T.; Lupulescu, C.; Minemoto, S.; Rosendo-Francisco, P.; Woste, L. *Chem. Phys.* **2001**, *267*, 231.
(34) Daniel, C.; Full, J.; Gonzalez, L.; Kaposta, C.; Krenz, M.; Lupulescu, C.; Manz, J.; Minemoto, S.; Oppel, M.; Rosendo-Francisco, P.; Vajda, S.; Woste, L. *Chem. Phys.* **2001**, *267*, 247.
(35) Weinacht, T. C.; White, J. L.; Bucksbaum, P. H. *J. Phys. Chem. A* **1999**, *103*, 10166.
(36) Hornung, T.; Meier, R.; de Vivie-Riedle, R.; Motzkus, M. *Chem. Phys.* **2001**, *267*, 261.
(37) Moore, N. P.; Menkir, G. M.; Markevitch, A. N.; Graham, P.; Levis, R. J. The Mechanisms of Strong-Field Control of Chemical Reactivity Using Tailored Laser Pulses. In *Laser Control and Manipulation of Molecules*; Gordon, R. J., Ed.; ACS Symposium Series in Chemistry; American Chemical Society: Washington, DC, 2001.
(38) Cornaggia, C.; Lavancier, J.; Normand, D.; Morellec, J.; Agostini, P.; Chambaret, J. P.; Antonetti, A. *Phys. Rev. A* **1991**, *44*, 4499.
(39) DeWitt, M. J.; Levis, R. J. *Phys. Rev. Lett.* **1998**, *81*, 5101.
(40) Markevitch, A. N.; Moore, N. P.; Levis, R. J. *Chem. Phys.* **2001**, *267*, 131.
(41) Hay, N.; Castillejo, M.; de Nalda, R.; Springate, E.; Mendham, R. J.; Marangos, J. P. *Phys. Rev. A* **2000**, *6105*, 3810.
(42) Bandrauk, A. D.; Ruel, J. *Phys. Rev. A* **1999**, *59*, 2153.
(43) Bandrauk, A. D.; Chelkowski, S. *Chem. Phys. Lett.* **2001**, *336*, 518.
(44) Bandrauk, A. D.; Chelkowski, S. *Phys. Rev. Lett.* **2000**, *84*, 3562.
(45) Keldysh, L. V. *Sov. Phys. JETP* **1965**, *20*, 1307.
(46) Perelomov, A. M. P.; V. S.; Terent'ev, M. V. *Sov. Phys. JETP* **1966**, 924.
(47) Ammosov, M. V. D., N. B.; Krainov, V. P. *Sov. Phys. JETP* **1986**, 1191.
(48) DeWitt, M. J.; Levis, R. J. *J. Chem. Phys.* **1998**, *108*, 7045.
(49) DeWitt, M. J.; Levis, R. J. *J. Chem. Phys.* **1999**, *110*, 11368.
(50) DeWitt, M. J.; Prall, B. S.; Levis, R. J. *J. Chem. Phys.* **2000**, *113*, 1553.
(51) Lezius, M.; Blanchet, V.; Rayner, D. M.; Villeneuve, D. M.; Stolow, A.; Ivanov, M. Y. *Phys. Rev. Lett.* **2001**, *86*, 51.
(52) Moore, N. P.; Levis, R. J. *J. Chem. Phys.* **2000**, *112*, 1316.
(53) Pan, L.; Armstrong, L.; Eberly, J. H. *J. Opt. Soc. Am. B* **1986**, *3*, 1319.
(54) Bucksbaum, P. H.; Freeman, R. R.; Bashkansky, M.; McIlrath, T. J. *J. Opt. Soc. Am B* **1987**, *4*, 760.
(55) Freeman, R. R.; Bucksbaum, P. H. *J. Phys. B* **1991**, *24*, 325.
(56) Moore, N. P.; Markevitch, A. N.; Levis, R. J. *J. Chem. Phys.* **2001**/**2002**, submitted.
(57) Muth-Bohm, J.; Becker, A.; Chin, S. L.; Faisal, F. H. M. *Chem. Phys. Lett.* **2001**, *337*, 313.
(58) Mukamel, S.; Tretiak, S.; Wagersreiter, T.; Chernyak, V. *Science* **1997**, *277*, 781.
(59) Tretiak, S.; Chernyak, V.; Mukamel, S. *Phys. Rev. Lett.* **1996**, *77*, 4656.
(60) Tretiak, S.; Chernyak, V.; Mukamel, S. *Chem. Phys. Lett.* **1996**, *259*, 55.
(61) Yu, H. T.; Zuo, T.; Bandrauk, A. D. *J. Phys. B* **1998**, *31*, 1533.
(62) Yu, H. T.; Bandrauk, A. D. *Phys. Rev. A* **1997**, *56*, 685.
(63) Zuo, T.; Bandrauk, A. D. *Phys. Rev. A* **1995**, *52*, R2511.
(64) Chelkowski, S.; Conjusteau, A.; Zuo, T.; Bandrauk, A. D. *Phys. Rev. A* **1996**, *54*, 3235.
(65) Snyder, E. M.; Buzza, S. A.; Castleman, A. W. *Phys. Rev. Lett.* **1996**, *77*, 3347.
(66) Ledingham, K. W. D.; Singhal, R. P. *Int. J. Mass Spectrom. Ion Process.* **1997**, *163*, 149.
(67) Baumert, T.; Gerber, G. *Phys. Scripta* **1997**, *T72*, 53.
(68) Zewail, A. H. *Phys. Today* **1980**, *33*, 27.
(69) Sokolov, A. V.; Walker, D. R.; Yavuz, D. D.; Yin, G. Y.; Harris, S. E. *Phys. Rev. Lett.* **2001**, *8703*, 3402.
(70) Peirce, A. P.; Dahleh, M. A.; Rabitz, H. *Phys. Rev. A* **1988**, *37*, 4950.
(71) Shi, S. H.; Woody, A.; Rabitz, H. *J. Chem. Phys.* **1988**, *88*, 6870.
(72) Shi, S. H.; Rabitz, H. *J. Chem. Phys.* **1990**, *92*, 364.
(73) Rabitz, H.; Zhu, W. S. *Acc. Chem. Res.* **2000**, *33*, 572.
(74) Gross, P.; Neuhauser, D.; Rabitz, H. *J. Chem. Phys.* **1993**, *98*, 4557.
(75) Toth, G. J.; Lorincz, A.; Rabitz, H. *J. Chem. Phys.* **1994**, *101*, 3715.
(76) Phan, M. Q.; Rabitz, H. *Chem. Phys.* **1997**, *217*, 389.
(77) Toth, J.; Li, G. Y.; Rabitz, H.; Tomlin, A. S. *Siam. J. Appl. Math.* **1997**, *57*, 1531.
(78) Toth, G. J.; Lorincz, A.; Rabitz, H. *J. Mod. Opt.* **1997**, *44*, 2049.
(79) Phan, M. Q.; Rabitz, H. *J. Chem. Phys.* **1999**, *110*, 34.
(80) Geremia, J. M.; Zhu, W. S.; Rabitz, H. *J. Chem. Phys.* **2000**, *113*, 10841.
(81) Geremia, J. M.; Weiss, E.; Rabitz, H. *Chem. Phys.* **2001**, *267*, 209.
(82) de Vivie-Riedle, R.; Sundermann, K.; Motzkus, M. *Faraday Discuss.* **1999**, 303.
(83) de Vivie-Riedle, R.; Sundermann, K. *Appl. Phys. B* **2000**, *71*, 285.
(84) Hornung, T.; Motzkus, M.; de Vivie-Riedle, R. *J. Chem. Phys.* **2001**, *115*, 3105.
(85) Kosloff, R.; Rice, S. A.; Gaspard, P.; Tersigni, S.; Tannor, D. J. *Chem. Phys.* **1989**, *139*, 201.
(86) Rice, S. A.; Zhao, M. *Optical Control of Molecular Dynamics*; John Wiley and Sons: New York, 2000.
(87) Rabitz, H.; Shi, S. In *Advances in Molecular Vibrations and Collision Dynamics*; JAI Press: New York, 1991; Vol. 1.
(88) Kunde, J.; Baumann, B.; Arlt, S.; Morier-Genoud, F.; Siegner, U.; Keller, U. *Appl. Phys. Lett.* **2000**, *77*, 924.
(89) Omenetto, F. G.; Taylor, A. J.; Moores, M. D.; Reitze, D. H. *Opt. Lett.* **2001**, *26*, 938.
(90) Turinici, G.; Rabitz, H. *Chem. Phys.* **2001**, *267*, 1.
(91) Ramakrishna, V.; Salapaka, M. V.; Dahleh, M.; Rabitz, H.; Peirce, A. *Phys. Rev. A* **1995**, *51*, 960.
(92) Brumer, P.; Shapiro, M. *Acc. Chem. Res.* **1989**, *22*, 407.
(93) Gross, P.; Rabitz, H. *J. Chem. Phys.* **1996**, *105*, 1299.
(94) Tannor, D. J.; Rice, S. A. *J. Chem. Phys.* **1985**, *83*, 5013.
(95) Shi, S. H.; Rabitz, H. *J. Chem. Phys.* **1992**, *97*, 276.
(96) Gaubatz, U.; Rudecki, P.; Schiemann, S.; Bergmann, K. *J. Chem. Phys.* **1990**, *92*, 5363.
(97) Rice, S. A.; Shah, S.; Tannor, D. J. *Abstr. Pap. Am. Chem. Soc.* **2000**, *220*, 280.
(98) Bryson, A. E. *Applied Optimal Control*; Hemisphere Publishing Corporation: Washington DC, 1975.
(99) Ohtsuki, Y.; Nakagami, K.; Fujimura, Y.; Zhu, W. S.; Rabitz, H. *J. Chem. Phys.* **2001**, *114*, 8867.
(100) Demiralp, M.; Rabitz, H. *Phys. Rev. A* **1993**, *47*, 831.
(101) Judson, R. S.; Lehmann, K. K.; Rabitz, H.; Warren, W. S. *J. Mol. Struct.* **1990**, *223*, 425.
(102) Shi, S. H.; Rabitz, H. *Chem. Phys.* **1989**, *139*, 185.

(103) Amstrup, B.; Carlson, R. J.; Matro, A.; Rice, S. A. *J. Phys. Chem.* **1991**, *95*, 8019.
(104) Tannor, D. J.; Kosloff, R.; Rice, S. A. *J. Chem. Phys.* **1986**, *85*, 5805.
(105) Shi, S.; Rabitz, H. *Comput. Phys. Commun.* **1991**, *63*, 71.
(106) Gross, P.; Ramakrishna, V.; Vilallonga, E.; Rabitz, H.; Littman, M.; Lyon, S. A.; Shayegan, M. *Phys. Rev. B* **1994**, *49*, 11100.
(107) Beumee, J. G. B.; Rabitz, H. *J. Math. Chem.* **1993**, *14*, 405.
(108) Weiner, A. M. *Prog. Quantum Electron.* **1995**, *19*, 161.
(109) Zeidler, D.; Hornung, T.; Proch, D.; Motzkus, M. *Appl. Phys. B* **2000**, *70*, S125.
(110) Bergt, M.; Brixner, T.; Kiefer, B.; Strehle, M.; Gerber, G. *J. Phys. Chem. A* **1999**, *103*, 10381.
(111) Brixner, T.; Kiefer, B.; Gerber, G. *Chem. Phys.* **2001**, *267*, 241.
(112) Goldberg, D. E. *Genetic Algorithms in Search, Optimization & Machine Learning*; Addison-Wesley Longman, Incorporated: Reading, MA, 1989.
(113) Pearson, B. J.; White, J. L.; Weinacht, T. C.; Bucksbaum, P. H. *Phys. Rev. A* **2001**, *6306*, 3412.
(114) Zeidler, D.; Frey, S.; Kompa, K. L.; Motzkus, M. *Phys. Rev. A* **2001**, *6402*, 3420.
(115) Rabitz, H.; Alis, O. F. *J. Math. Chem.* **1999**, *25*, 197.
(116) Geremia, J. M.; Rabitz, H.; Rosenthal, C. *J. Chem. Phys.* **2001**, *114*, 9325.
(117) Berkowitz, J.; Ellison, G. B.; Gutman, D. *J. Phys. Chem.* **1994**, *98*, 2744.
(118) Zhu, W. S.; Rabitz, H. *J. Chem. Phys.* **1999**, *111*, 472.
(119) Lu, Z. M.; Rabitz, H. *Phys. Rev. A* **1995**, *52*, 1961.